# Hydrogen-Induced Calcium Influx via the TRPC4-TRPC4AP Axis

**Pengxiang Zhao[1,]*, Han Li[1,] *, Zisong Cai[1,] ***, Xujuan Zhang[1], Xiaohu Wen[1], Ziyi Liu[1], Shihao Jiang[1], Zheng Dang[1], Xue Jiang[1], Jiateng Wang[1], Mengyu Liu[1], Fei Xie[1], and **Xuemei Ma[1, #]**

[1]College of Chemistry and Life Science, Beijing University of Technology, Beijing 100124, P. R. China

**# Correspondence: Xuemei Ma, xmma@bjut.edu.cn**

*** These authors share first authorship**

**Abstract**：

**Background:** Calcium ions ($Ca^{2+}$) serve as universal intracellular messengers regulating diverse physiological processes, while dysregulated $Ca^{2+}$ homeostasis triggers cytotoxicity. Molecular hydrogen ($H_2$) exhibits protective effects against oxidative stress-related pathologies, but its mechanism of action remains incompletely understood. Transient receptor potential canonical 4 (TRPC4) channels and their associated protein TRPC4AP are critical mediators of $Ca^{2+}$ influx ( $[Ca^{2+}]i$), yet their role in $H_2$-mediated calcium signaling is unexplored. This study investigates the molecular mechanism by which $H_2$ modulates $Ca^{2+}$ dynamics through the TRPC4-TRPC4AP axis, aiming to establish its therapeutic potential for calcium-related disorders.

**Methods:** The study employed heterogeneous cellular models (e.g., mesenchymal stem cells, neurons, fibroblasts) and in vivo two-photon calcium imaging in C57BL/6J mice. Techniques included CRISPR-Cas9 knockout, siRNA-mediated gene silencing, molecular docking (AlphaFold 3), and protein-protein interaction analysis. Calcium flux was quantified via fluorescence imaging, while mitochondrial integrity and cytoskeletal dynamics were assessed using JC-1 staining, ATPase activity assays, and live-cell imaging. Structural validation of TRPC4-TRPC4AP binding sites utilized mutagenesis and complementation experiments.

**Results:** $H_2$ selectively enhanced extracellular $Ca^{2+}$ influx via TRPC4-TRPC4AP, with no cytotoxicity or mitochondrial dysfunction observed. Key arginine residues (730Arg-731Arg) in the TRPC4 CIRB domain formed hydrogen-bond networks essential for channel activation. In vivo, $H_2$ increased neuronal $Ca^{2+}$ transient frequency and amplitude in the primary motor cortex. TRPC4AP knockout abolished $H_2$-induced $Ca^{2+}$ influx, while mutagenesis of 730Arg/731Arg disrupted channel activity. $H_2$ also promoted cytoskeletal remodeling and cell motility, dependent on TRPC4AP-mediated $Ca^{2+}$ signaling.

**Conclusions:** This study identifies $H_2$ as a novel calcium agonist that activates the TRPC4-TRPC4AP axis to regulate extracellular $Ca^{2+}$ influx. The 730Arg-731Arg motif in TRPC4 serves as a critical $H_2$-sensitive site, enabling dynamic calcium homeostasis without overload. These findings provide a mechanistic basis for $H_2$-based therapies targeting calcium dysregulation in neurodegenerative, inflammatory, and metabolic diseases, while highlighting TRPC4AP as a pivotal molecular switch for gasotransmitter signaling.

**Key Wrods**

Calcium Ion; Molecular Hydrogen; TRPC4; TRPC4AP; Calcium Agonist.

## Introduction

Calcium ions ($Ca^{2+}$) function as a ubiquitous second messenger, mediating various physiological processes through dynamic concentration gradients and complex regulatory mechanisms[1]. Cytoplasmic calcium elevation serves as a universal signaling pathway[2], transmitting signals from the cell surface to the interior, regulating key cellular functions, including gene expression[3], cell cycle progression[4], motility[5], autophagy[6], and apoptosis[7]. In the nervous system, $Ca^{2+}$ is essential for neurotransmitter release, facilitating neuronal communication[8], while in muscle cells, it is critical for contraction by interacting with regulatory proteins like troponin to enable actin-myosin interaction and force generation[9]. $Ca^{2+}$ also activate numerous enzymes, such as thrombin, which is involved in blood clotting[10]. Additionally, extracellular $Ca^{2+}$ maintains the resting membrane potential in excitable cells, such as neurons and muscle cells, and supports proper bone formation[11].

Cytoplasmic $Ca^{2+}$ signals arise from extracellular calcium influx through calcium channels. The endoplasmic reticulum (ER) and mitochondria (Mito) serve as key intracellular calcium reservoirs[12, 13]. In the ER, calcium ions are vital for proper protein folding, and their release via calcium channels contributes to cytoplasmic calcium signaling[14]. Mitochondria play a crucial role in shaping these signals through their calcium transport mechanisms[15].

Intracellular calcium concentrations exhibit dynamic fluctuations, typically ranging from 20 nM to 2 μM, depending on cellular activity[12]. In resting cells, calcium levels are tightly regulated below 200 nM, which is significantly lower than the extracellular concentration (~1 mM) and the luminal calcium stores in the SR/ER (100–500 μM)[16]. This steep electrochemical gradient is maintained by two primary calcium extrusion mechanisms: the plasma membrane calcium ATPase (PMCA) and the sodium-calcium exchanger (NCX), which cooperate to expel calcium from the cytoplasm[17]. The extracellular space serves as an abundant reservoir for calcium, facilitating its influx into the cytoplasm through various channels, including store-operated, voltage-gated, ligand-gated, and TRP channels. In non-excitable cells, store-operated calcium entry (SOCE) is the predominant pathway, activated upon depletion of ER calcium stores[18]. Additionally, voltage-gated and ligand-gated channels mediate calcium entry in response to changes in membrane potential or ligand binding, respectively[8].

This article focuses on TRP channels, specifically the TRPC family. TRPC channels are permeable to monovalent and divalent cations, including $Na^{+}$, $K^{+}$, $Ca^{2+}$, and $Zn^{2+}$. Among the four subgroups of TRPC channels, three (TRPC1, TRPC4-TRPC5, and TRPC3-TRPC6-TRPC7) form heteromeric complexes in humans[19, 20]. Each TRPC subunit comprises six transmembrane segments that form the cation-permeable pore.The regulation of TRPC channels is influenced by post-translational modifications (e.g., phosphorylation and glycosylation) and specific domains in the N and C termini of the subunits, such as coiled-coil domains, ankyrin repeat domains, calmodulin-binding sites, and binding sites for the inositol 1,4,5-trisphosphate receptor (IP3R1)[21]. TRPC channels can be activated by G protein-coupled receptors (GPCRs) or oxidative stress and are sensitive to changes in intracellular osmolarity or $Ca^{2+}$ levels[20].

Calcium agonists are compounds that increase $Ca^{2+}$ influx into calcium channels in excitable tissues, which is crucial for functions like muscle contraction, vascular regulation, and hormone release[22]. These agonists may have therapeutic potential for treating degenerative diseases, such as amyotrophic lateral sclerosis[23]. However, there are far fewer identified calcium channel agonists compared to the many calcium channel antagonists.

$H_2$ is small, non-polar, and highly permeable, enabling it to cross cellular membranes and enter organelles, facilitating interactions with crucial cellular components. Ohta et al. found that 2% $H_2$ can effectively reduce cerebral ischemia-reperfusion injury in rats, suggesting a selective antioxidant mechanism[24]. Despite its protective effects against various oxidative stress-related diseases, the traditional antioxidant hypothesis does not fully explain the diverse biological effects of $H_2$, leading to further exploration of its mechanisms[25].

Our research has revealed that $H_2$ acts as a calcium ion agonist through the TRPC4 channel and its associated protein, TRPC4-associated protein (TRPC4AP), promoting the influx of extracellular $Ca^{2+}$ into cells and thereby increasing the concentration of calcium ions in the cytoplasm[26]. This effect is widely applicable across various cell types, triggering biological responses in a multitude of cellular contexts. The increase in cytoplasmic calcium ion concentration induced by hydrogen gas stimulation is reversible and does not lead to calcium overload or reduced cell viability. TRPC4AP does not directly constitute the ion channel but serves as a functional partner protein of TRPC4, influencing TRPC4-dependent calcium signaling pathways by regulating its expression levels, subcellular localization, or channel activity.

To elucidate the molecular mechanism of $H_2$-induced extracellular $Ca^{2+}$ influx, this study employed siRNA-mediated gene silencing technology for functional validation. We demonstrated that this process is predominantly mediated by the TRPC4 channel localized on the plasma membrane and its interacting partner TRPC4AP. Utilizing the AlphaFold 3 structural prediction platform combined with protein-protein molecular docking techniques, we systematically resolved the three-dimensional conformation of the TRPC4-TRPC4AP complex[27]. Structural simulations and statistical analyses revealed, for the first time, that TRPC4AP regulates channel activity by specifically binding to the CIRB domain (Calmodulin/IP3 Receptor Binding Domain) of the TRPC4 protein. Molecular dynamics investigations further demonstrated that $H_2$ modulates channel activity by targeting the CIRB domain within the TRPC4-TRPC4AP complex. Notably, the arginine residues at positions 730 (Arg730) and 731 (Arg731) of TRPC4 play a pivotal role in $H_2$-mediated $Ca^{2+}$ transmembrane transport by forming critical hydrogen-bond networks. These findings provide essential structural insights into the gating mechanism of the TRPC4/TRPC4AP complex and its functional role in gas signaling transduction.

This discovery positions TRPC4AP as a unique molecular target for hydrogen therapy, bridging the gap between its observed biological effects and mechanistic understanding. Our findings not only advance $H_2$ medicine research but also provide a framework for developing targeted therapies for degenerative diseases, while informing future investigations into $H_2$ dosing optimization and safety profiles.

**Materials and methods**

**Cellular Immunofluorescence Assay**

Cells were cultured on glass coverslips within a 6-well plate to the appropriate confluence. Aspirate the medium, wash with PBS, and fix cells with 4% paraformaldehyde for 15 minutes at room temperature. Permeabilize with 0.1% Triton X-100 for 10 minutes, then block with 3% BSA in PBS for 1 hour. Incubate with the primary antibody overnight at 4°C, followed by three washes with PBS. Apply the fluorophore-conjugated secondary antibody for 1 hour at room temperature in the dark, and wash again. Stain nuclei with DAPI for 5 minutes, then mount the coverslips on slides with mounting medium. Analyze the cells using Confocal Fluorescence Microscopy (Nicon, C2, Japan ), ensuring to protect the samples from light to prevent photobleaching.

**Preparation of Cell Samples for TEM**

Harvest and Centrifuge cultured cells to form a pellet, then immediately fix the cells in a solution of 2% glutaraldehyde and 2% paraformaldehyde in PBS for 2 hours at 4°C. Wash the pellet with sodium cacodylate buffer, followed by post-fixation in 1% osmium tetroxide. Dehydrate the sample through an ascending ethanol series and transition with propylene oxide. Infiltrate and embed the sample in resin, then polymerize at 60-70°C. Trim and section the embedded block with an ultramicrotome to obtain ultrathin sections. Stain the sections with uranyl acetate and lead citrate, mount them on copper grids, and examine the cellular ultrastructure using a transmission electron microscope (HITACHI, HT7700, Japan).

**Mitochondrial membrane potential detection JC-1**

293T cells were seeded at a density of $5\times10^3$cells per well in a 96-well plate, with the experimental group receiving culture medium saturated with hydrogen gas. After 24 hours of cell adhesion, when the cell density reached approximately 90%, the cells were used to observe the mitochondrial membrane potential. The culture plate was removed and the cells were gently washed three times with PBS solution to remove impurities from the culture medium. To each well, 200 μL of JC-1 staining working solution with a final concentration of 2 μM was added.The plate was then placed back into the cell incubator and incubated at 37°C for 20 minutes to allow sufficient staining of the mitochondria with JC-1 dye. After incubation, the supernatant was carefully aspirated, and the cells were washed three times with JC-1 staining buffer to remove any unbound dye.200 μL of cell culture medium was added back to each well to maintain the physiological state of the cells. The cells were observed and the fluorescence staining results were recorded using a laser confocal microscope to assess changes in the mitochondrial membrane potential.

**Cell viability assay**

The cell viability of the 293T cell line was assessed using the Cell Counting Kit-8 (CCK8). These cells were seeded at a density of $5\times10^3$ cells per well in a 96-well plate,

and after growing for 24 hours in standard growth medium, the medium was replaced with medium saturated with hydrogen gas. The cell viability was detected using the CCK8 reagent at 2h, 4h, 8h, and 24h time points. The optical density (OD) was measured at 450 nm using a Perkin Elmer microplate reader.

The blank group contained only the culture medium, the control group contained cells that were not treated with saturated hydrogen gas, and the positive control group contained cells treated with 2μM ionomycin to induce calcium overload.

Cell viability = (Abs of the experimental group-Abs of the blank group)/(Abs of the control group-Abs of the blank group) ×100 %.

**Cell death rate assessment and live cell imaging**

NucGreen Dead 488 Ready Probes Reagent (ThermoFisher S7020) is a membrane-impermeable stain that selectively labels cells with compromised membranes by binding to DNA and emitting a vivid green fluorescence, without penetrating or affecting the integrity of living cells. This reagent is used to quantify the relative rate of cell death according to the guidelines provided by Thermo Fisher Scientific.

Live cell imaging is a powerful tool for capturing the dynamics of cellular processes and events. Images of 293T cells were captured using the Cytation 5 Cell Imaging Multimode Reader (Biotek Instruments, Inc.,Winooski, VT, USA).Cells were treated with NucGreen Dead 488 Ready Probes Reagent to observe the number of live and dead cells after hydrogen treatment at 2h, 4h, 8h, and 24h time points. The cell imaging data were processed and cell counts were analyzed using Gen5™ Data Analysis Software from Bad Friedrichshalle, Germany.

The control group contained cells that were not treated with saturated hydrogen gas, and the positive control group contained cells treated with 75% ethanol.

**Ca++Mg++-ATPase Activity Assay**

Ca++Mg++-ATPase enzymes are widely distributed in plants, animals, microorganisms, and cells, and can catalyze the hydrolysis of ATP to produce ADP and inorganic phosphate. Ca++Mg++-ATPase Assay Kit (Bioss AK266) utilizes the principle of Ca++Mg++-ATPase decomposing ATP to generate ADP and inorganic phosphate, and determines the activity of ATPase by measuring the amount of inorganic phosphate. 293T cells were seeded at a density of $10^5$ cells/mL in T25 flasks and grown in standard growth medium for 24 hours before being replaced with medium saturated with hydrogen gas. After 5 and 10 minutes, the activity of Ca++Mg++-ATPase was determined using the assay kit. The control group contained cells that were not treated with saturated hydrogen gas. The optical density (OD) was measured at 660 nm using a Perkin Elmer microplate reader.

Ca++Mg++-ATPase activity (μmol/h/$10^4$) = 0.015 × (A of the test tube - A of the control tube) ÷ (A of the standard tube - A of the blank tube).

**Cell scratch assay**

A confluent monolayer of cells was seeded in a 6-well plate. Once confluent, remove the medium and gently scratch the cell layer uniformly across the well with a pipette tip to create a 'wound.' Wash the cells with PBS to remove any debris and floating cells. Add fresh culture medium, and return the plate to the Live cell imaging system (Biotek Instruments, Inc., Winooski, VT, USA). Capture images of the wound area at the start and at regular time intervals automaticly. After the experiment, analyze the images to measure the rate of cell migration into the wound area over time. The wound healing rate can be quantified by comparing the wound area at different time points, indicating cell migration and proliferation capabilities.

**$Ca^{2+}$, $K^{+}$, $Na^{+}$ ion probe staining and imaging in live cells**

Cells were seeded on glass coverslips in a culture dish to reach the desired confluence. Wash the cells gently with warm Hank's Balanced Salt Solution (ThermoFisher 14175095) to remove culture medium. Incubate the cells with an ion sensitive fluorescent Probe for $Ca^{2+}$-Fluo-4-AM (5 μM ) diluted in Serum-Free Medium (KeyGEN,KGAF024) ; Probe for $K^{+}$-EPG-4-AM (5 μ M) diluted in Serum-Free Medium(Maokang MX4521) ; Probe for $Na^{+}$-ENG-2-AM (5 μ M ) diluted in Serum-Free Medium(Maokang MX4514) ; probe for $Ca^{2+}$-Rhod-2-AM (5 μM ) diluted in HBSS(YEASEN 40776ES72) for 10-30 min at 37°C to allow probe uptake. After incubation, wash off excess probe with HBSS or Serum-Free Medium and place the cells in a recording chamber for microscopy. Confocal microscope equipped with a CCD camera (C2, Nicon) was used to capture the fluorescence signal, which indicates ion concentration. Maintain the cells at 37°C and control the atmosphere ($CO_2$ level) throughout the imaging process to keep the cells viable, and monitor calcium dynamics in response to stimuli. Analyze the fluorescence intensity changes to assess ion activity within the cells.

**Western blot**

Cells were washed, harvested, and centrifuged, and proteins were extracted using a Cell Protein Extraction Kit (San Gong, C006225). All procedures were carried out on ice. After cell lysis, protein quantification was performed using the BCA Protein Assay Kit (Beyotime P0010). Equal amounts of cell protein samples were separated by 10% sodium dodecyl sulfate-polyacrylamide gel electrophoresis (SDS-PAGE) and transferred onto a nitrocellulose membrane (Millipore). The membrane was blocked with a 3% BSA blocking solution for 2 hours at room temperature, then washed three times with TBST, and incubated with the target primary antibody overnight at 4°C. After incubation with a fluorophore-conjugated secondary antibody for 1 hour in the dark, the bands were visualized and captured using the LI-COR® Odyssey Infrared Imaging

System.

**Lipofectamine 2000 transfection of siRNA**

Cells were seeded at a density of $5\times10^3$ cells/well in a 96-well plate and cultured in standard growth medium for 24 hours. On the day of transfection, cells were seeded in an appropriate amount of growth medium without antibiotics to achieve a confluence of 30-50% at the time of transfection. siRNA was diluted in serum-free Opti-MEM (Gibco, 2898884), mixed gently, and Lipofectamine 2000 (ThermoFisher, 11668019) was diluted in Opti-MEM. The diluted siRNA and diluted Lipofectamine 2000 were mixed and incubated at room temperature for 20 minutes to form siRNA-Lipofectamine 2000 complexes. The siRNA-Lipofectamine 2000 mixture was added to each well containing cells and medium. The plate was gently rocked back and forth to mix. Cells were incubated in a 37°C $CO_2$ incubator for 48-96 hours, and the medium could be changed after 6-8 hours.

**Molecular Docking**

The initial structure of TRPC4 was obtained from the PDB database, with the entrance ID of 7B0J. In the absence of experimentally resolved TRPC4AP structures, we employed AlphaFold we employed AlphaFold to predict the full-length of this associated protein. we utilized SWISSMODEL to refine and complete the TRPC4 protein chain, thus ensuring its functional integrity. In subsequent research, the binding modes and detailed interactions between TRPC4 and TRPC4AP was investigated using protein-protein docking technology.

we generated 2,000 potential docking configurations between TRPC4 and TRPC4AP. Utilizing the PSC (Protein Scoring Function) scoring system, the software performed an automated clustering and scoring of these configurations, ultimately identifying the top 60 TRPC4 and TRPC4 AP binding modes. These initial docking models were based on a rigid docking approach, in an effort to refine these docking configurations ,we employed energy optimization to eliminate potential geometric conflicts in these docking conformations, laying a robust foundation for further experimental validation and clinical applications.

By utilizing advanced protein-docking software, we were not only able to simulate the binding process between TRPC4 and TRPC4AP but could also examine the specific interactions at their interfaces.

In a practical application of AlphaFold 3, we input the amino acid sequences of TRPC4 and TRPC4AP into the AlphaFold 3 platform to obtain a model of the TRPC4-TRPC4 AP complex. We analyzed the interfacial interactions within this complex. Notably, an interaction between arginine at position 730 on TRPC4 and a glutamic acid on TRPC4 AP, which received the highest score using the PSC. We have obtained results consistent with our previous protein-protein docking, which confirms that our analysis is correct.

**Construction and Identification of pX459-sgRNA Knockout Plasmids Targeting TRPC4 and TRPC4AP**

Based on the genomic information of TRPC4 and TRPC4AP genes from NCBI, the exons were annotated. The nucleotide sequences of the first and second exons of the

target genes were input into the sgRNA online design website http://crispr.mit.edu. Two sgRNA sequences with the lowest off-target rates were selected. After synthesis by Suzhou Hongxun Biotechnology Co., Ltd., they were named: TRPC4 sgRNA-1 and TRPC4 sgRNA-2; TRPC4 AP sgRNA-1 and TRPC4 AP sgRNA-2. The sgRNA primers were annealed to form double-stranded DNA through a programmable annealing process. The vector pX459 was linearized after digestion with BbsI enzyme and then recovered. T4 DNA ligase was used to ligate the annealed sgRNA double-stranded DNA with the linearized pX459 at room temperature to obtain the recombinant plasmids, which were then sequenced and identified for correctness before being used in subsequent experiments.

**Preparation and Selection of 293T Cells with TRPC4 and TRPC4AP Gene Knockout**

Seed HEK293T cells into a 6-well cell plate, and when the cell confluence reaches 80%, transfect the 293T cells with the pX459 plasmid carrying TRPC4 and TRPC4AP sgRNA. Meanwhile, transfect with empty plasmid pX459 in the same manner as a negative control. After 36 hours, perform pressure screening with 1μg/mL puromycin. After two rounds of puro selection, once the control group cells have all died, digest the experimental group cells into single cells, and use the limited dilution method to sort out monoclonal cells and expand the culture. After passaging the cell line, freeze and store for future use.

**Identification of Gene and Protein Knockout in 293T Cell Lines with TRPC4 and TRPC4AP Gene Knockout**

Collect monoclonal cell strains and number them. Extract the genomic DNA from the cells according to the instructions of the DNA extraction kit. Based on the genomic sequences of TRPC4 and TRPC4AP targeted by sgRNA, design specific identification primers according to the intron sequences on both sides of the corresponding exons. Use these primers and the extracted cellular genomic DNA as templates to perform PCR amplification. The amplified products are sequenced and aligned to detect the knockout effect of the target genes in the obtained monoclonal cell strains.

**Animal Studies**

Male C57BL/6J mice (8 weeks old) were obtained from Charles River Laboratories (Beijing). Mice were maintained in a 12-hour light/dark cycle at 25°C with free access to food and water. All animal experiments were approved by the Institutional Animal Care and Use Committee (IACUC) and were conducted in accordance with the guidelines for the ethical treatment of animals. To monitor $Ca^{2+}$ influx in the primary motor cortex (M1), C57BL/6J mice were stereotactically injected with adeno-associated virus (AAV) expressing Syn1-driven jGCaMP7 (AAV-Syn1-jGCaMP7).

Mice were anesthetized using isoflurane 2% in oxygen and positioned in a stereotactic frame. The scalp was shaved and disinfected with ethanol. A midline incision was made, and a small craniotomy (1-2 mm in diameter) was performed at the coordinates (X=2 mm lateral, Y=0.8 mm anterior, Z=2.4 mm depth) relative to bregma, to target the primary motor cortex (M1). AAV-Syn1-jGCaMP7 (titer: $1 \times 10^{13}$ vg/mL) was injected at a rate of 0.2 μL/min using a microinjection pump (UltraMicroPump3 (UMP3)). A total of 50 μL of AAV vector was delivered into M1. The needle was left in place for an additional 5 minutes to

allow for viral diffusion, and the incision was closed with sutures. Mice were allowed to recover for 2-3 weeks to ensure proper viral expression and cellular uptake.

**Two-Photon Microscopy for In Vivo Calcium Imaging in the Primary Motor Cortex (M1)**

Experimental Setup and Preparation To monitor real-time calcium dynamics in the primary motor cortex (M1) of C57BL/6J mice infected with AAV-Syn1-jGCaMP7, in vivo two-photon imaging was performed as follows:

Animal Preparation . After the recovery period post-surgery and sufficient expression of jGCaMP7 in the M1 region, mice were anesthetized with isoflurane (2% for induction, 1-1.5% for maintenance) and placed onto a custom imaging platform. Core body temperature was maintained at 37°C using a heating pad.

Cranial Window and Imaging Setup. A cranial window above the primary motor cortex was prepared by carefully removing the overlying skin and gently clearing the bone over M1. A round coverslip was placed on the exposed cortical surface to protect the brain tissue and reduce motion artifacts. The window was sealed with dental cement (C&B Metabond) to secure the coverslip in place.

Imaging Preparation. The mouse was placed under the objective lens of the two-photon microscope (Olympus FV1000, Leica SP8), and the brain region of interest was positioned in the imaging field. The system was equipped with a Ti:sapphire laser for two-photon excitation (900 nm), and the emitted fluorescence from jGCaMP7 was collected through a 510–550 nm bandpass filter.

**Bulk-RNA seq and analysis**

The raw RNA-seq data were processed using a standard pipeline by Annoryoda, and were then deeply analyzed and visualized using R (version 4.4.1). The script utilized in this study is provided in the supplemental materials. Differential expression genes were screened based on the criteria of an adjusted P-value < 0.05 and an absolute fold change > 2. Principal component analysis (PCA) was conducted to assess the overall variance in the dataset, and hierarchical clustering was performed to group samples according to their gene expression patterns. Heatmaps of the differentially expressed genes were generated using the pheatmap package. Gene ontology (GO) and Kyoto Encyclopedia of Genes and Genomes (KEGG) enrichment analyses were carried out on the differentially expressed genes using the clusterProfiler package, aiming to identify the biological processes and pathways that are enriched in the data. GSEA analysis was also performed to demonstrate the expression trends of all genes.

In detail, we conducted individual K-Means fuzzy clustering analyses to delineate the transcriptomic profiles of DEGs in MSCs exposed to $H_2$ for 2 hours (MSCs-2h-$H_2$) versus control conditions (MSCs-2h-Ctrl), and after 24 hours (MSCs-24h-$H_2$) versus control conditions (MSCs-24h-Ctrl). Subsequently, we performed an integrated K-Means clustering on the top 5000 DEGs identified from the aforementioned pairwise comparisons to elucidate the overarching transcriptional dynamics. GO enrichment analysis was subsequently applied to each distinct cluster to infer functional annotations and biological processes that were significantly enriched. Furthermore, we executed a temporal transcriptome analysis to track the evolution of gene expression patterns over the specified

time intervals, providing insights into the temporal regulation of MSCs in response to $H_2$.

## Results

### $H_2$ promotes the accumulation of $Ca^{2+}$ in the cytoplasm

$Ca^{2+}$, functioning as master intracellular secondary messengers, orchestrate cellular signaling networks and physiological processes through spatiotemporal concentration gradients. This study unveils a novel molecular mechanism whereby $H_2$ specifically activates cytosolic $Ca^{2+}$ signaling in a dynamically reversible manner. Systematic interrogation across eight heterogeneous cellular models (Fig 1, Fig 2). Including human umbilical cord-derived mesenchymal stem cells (MSCs) Fig. 1A; bone marrow-derived mesenchymal stem cells (iBMSCs) Fig. 2A, mouse osteoblasts (MC3T3-E1) Fig. 2B; mouse myoblasts (C2C12) Fig. 2C,; mouse fibroblasts (NIH-3T3) Fig. 2D,; human skin fibroblasts (ESF) Fig. 2E, and rat neuronal cells (PC12) Fig. 2F.

We revealed that $H_2$-induced $Ca^{2+}$ mobilization exhibits graded concentration-dependent responsiveness. Taking human umbilical cord derived mesenchymal stem cells (MSCs) as an example, a paradigmatic model, $H_2$ exposure triggered rapid $Ca^{2+}$ elevation ($\Delta F/F_0$ = 2.8 ± 0.3 within 30 s; Fig 1A, Fig 1B), with signal intensity returning to baseline upon $H_2$ removal (Fig 1C, Fig 1D, Figure S1A). Strikingly, spontaneous resurgence of calcium oscillations—a conserved signaling modality characterized by periodic $Ca^{2+}$ fluctuations was observed approximately 50 minutes post-$H_2$ withdrawal (Fig. 1E). Concentration-gradient experiments further demonstrated a 42.7% ± 5.1% reduction in $Ca^{2+}$ fluorescence intensity when $H_2$ concentration decreased from saturation (1.6 ppm) to half-saturation (0.8 ppm) (Fig. 1F). Crucially, this regulatory mechanism operated independently of oxygen tension (Figure. S1B), suggesting $H_2$ modulates calcium homeostasis through non-canonical pathways, potentially involving TRPC4/TRPC4AP complex targeting.

### Extracellular $Ca^{2+}$ account for $H_2$-induced cytoplasmic $Ca^{2+}$ accumulation

Cytosolic $Ca^{2+}$ accumulation may originate from three principal sources: extracellular influx, release from ER calcium reservoirs, or mitochondrial calcium discharge. Our investigations demonstrated that $H_2$ had no significant effect on cytosolic $Ca^{2+}$ under $Ca^{2+}$-free medium conditions. Remarkably, upon reintroduction of $Ca^{2+}$-containing medium, $H_2$ regained its capacity to accumulate $Ca^{2+}$ in the cytoplasm, with the fluorescence intensity ratio ($F/F_0$) recovering to 92.4% ± 6.7% (Fig. 1G; Fig.1H). To investigate the role of ER calcium stores in $H_2$ induced calcium signaling, we employed pharmacological calcium depletion using 2-aminoethoxydiphenyl borate (2-APB). Experimental results demonstrated that even under ER calcium store-specific depletion conditions, $H_2$ still significantly elevated cytosolic $Ca^{2+}$ concentrations (Fig. 1I; Fig.1J). Using fluorescence probes specifically targeting ER and mitochondrial calcium, quantitative analysis via dual-channel ratiometric fluorescence imaging revealed no significant changes in calcium levels within the ER or mitochondria under $H_2$ exposure. Colocalization of mitochondrial calcium (Mito-$Ca^{2+}$) and endoplasmic reticulum calcium (ER-$Ca^{2+}$) with their respective calcium indicators(Fig. 1M). A simplified model illustrating how $H_2$ promotes the increase of intracellular calcium ([$Ca^{2+}$]i) through the influx of extracellular calcium (Fig. 1N).Statistical analysis of calcium source contributions

based on fluorescence intensity further indicated that the observed increase in intracellular calcium signals primarily originated from extracellular calcium influx, while ER calcium release exhibited minimal contribution. These findings confirm the dominant role of extracellular calcium entry in mediating $H_2$-regulated calcium homeostasis.

**Broad-Spectrum $Ca^{2+}$ Accumulation in the Cytoplasm Induced by $H_2$**

To validate the broad-spectrum effects of $H_2$ , we initially investigated its impact on human umbilical vein endothelial cells (HUVECs) (Figure S2). Our findings revealed that hydrogen gas induced cytoplasmic calcium ion ($Ca^{2+}$) accumulation in HUVECs, with a more rapid decline rate compared to mesenchymal stem cells (MSCs) (Figure. S2A, Figure. S2B). This hydrogen-induced calcium elevation exhibited reversibility, as calcium concentrations returned to baseline levels following replacement with hydrogen-free standard medium (Figure. S2A, Figure. S2B). Notably, similar to observations in MSCs, the hydrogen-triggered calcium increase in HUVECs showed minimal dependence on endoplasmic reticulum (ER) calcium stores, with extracellular calcium influx playing a predominant role. This conclusion was supported by both ER calcium store inhibitor experiments (Figure. S2C, Figure. S2D) and calcium-free medium tests (Figure. S2E, Figure. S2F) in HUVECs.

Expanding our investigation to diverse cell types, we observed varying magnitudes of hydrogen-induced cytoplasmic calcium elevation across multiple cellular models, including iBMSCs (Fig. 2A); MC3TE-e1 (Fig. 2B); C2C12 (Fig. 2C), NIH-3T3 (Fig. 2D), ESF (Fig. 2E), and PC12 (Fig. 2F). These collective results demonstrate the universal efficacy of hydrogen gas in promoting calcium influx across distinct cell types.

To further validate the regulatory effect of hydrogen on intracellular $Ca^{2+}$ in vivo, we employed two-photon in vivo calcium imaging (Fig. 2G). C57BL/6J mice received stereotaxic injections of AAV-Syn1-jGCaMP7 into the primary motor cortex (M1) for neuron-specific calcium indicator expression. Quantitative analysis of 15 neuronal cells in the M1 region (Fig. 2H) revealed that hydrogen inhalation (HI) significantly increased the frequency of calcium transients compared to the control group (CTL), with mean hourly peak counts of 50 versus 25 respectively (Fig. 2I). Moreover, hydrogen exposure enhanced the maximum calcium signal amplitude (CTL: 22,000 ± 500 vs. HI: 23,000 ± 450) (Fig. 2J). These in vivo findings closely aligned with our previous cellular experimental observations, collectively demonstrating that hydrogen effectively promotes calcium influx in both in vivo and in vitro systems.

**$H_2$ Promotes $Ca^{2+}$ Influx without Inducing Mt $Ca^{2+}$ Overload**

High levels of intracellular $Ca^{2+}$ can lead to severe cytotoxicity, particularly in the regulation of mitochondria, where $Ca^{2+}$ enter and exit through a variety of specialized channels and transporters in a tissue-specific manner. Relatively low levels of $Ca^{2+}$ concentration are necessary for mitochondrial energy metabolism, while excessive mitochondrial calcium can directly destroy energy metabolism and lead to apoptosis. Calcium overload is an intermediate state that can disrupt oxidative phosphorylation and is associated with multiple organ dysfunctions. We used ionomycin as a positive control for calcium overload and performed CCK8 assays, which showed that cell viability of MSCs at 24-hour, and 293T at 4-hour, 8-hour, and 24-hour time points was higher in the

$H_2$ group than in the ionomycin group, with no significant difference from the control group (Fig. 3A, Fig. 3G).

JC-1 staining indicated that after 24 hours of $H_2$ treatment, the mitochondrial membrane potential was not significantly different from the control group (Fig. 3B, Fig.3C, and Fig.3H), indicating that mitochondrial function was unaffected. After $H_2$ treatment for 2 hours and 24 hours, there was a noticeable increase in the number of rod-shaped mitochondria and the total mitochondrial count in MSCs (Fig.3D, Fig.3E and Fig.3F), suggesting an enhancement of mitochondrial energy metabolism by $H_2$. $H_2$ treatment, which is a single treatment, can affect $Ca^{2+}$ influx as the $H_2$ concentration in the culture medium decreases. After a single treatment of 293T cells with $H_2$ for 2630 seconds, the intracellular $Ca^{2+}$ concentration basically returned to the level of the control group (Fig. 3J, Fig. 3K), suggesting that $Ca^{2+}$ may also be actively pumped out. Further measurement of Ca-Mg-ATPase activity at different time points revealed that the enzyme activity in the $H_2$ group increased over time, showing a gradually rising trend (Fig. 3L), and reached more than six times that of the control group after 30 minutes. Another channel for calcium extrusion at the cell membrane is NXC, and since the $Na^+$ concentration did not change significantly (Figure. S3B, Figure. S3D), the role of this channel in calcium extrusion is excluded. In addition, after a single treatment with $H_2$, the endoplasmic reticulum $Ca^{2+}$ slightly increased (Fig. 1 K), possibly because the ER stored the excess $Ca^{2+}$ from the cytoplasm. In summary, the calcium influx induced by hydrogen treatment can be avoided by extrusion through cell membrane-related channels or storage in the ER, preventing excessive calcium in the cytoplasm and thus avoiding calcium overload.

**TRPC4 Channel: A Pathway for $H_2$-Promoted $Ca^{2+}$ Influx and Its High Dependency on TRPC4AP Protein**

Through transcriptome sequencing analysis, we systematically compared FPKM values of calcium channel-related genes in MSC membranes, revealing predominant expression of T-type, L-type, and N-type voltage-gated calcium channels (VGCCs) (Figure. S4A). Among transient receptor potential (TRP) channels, TRPM4, TRPM7, TRPV2, TRPC1, and TRPC4 showed prominent expression (Figure. S4B), with TRPC4AP being the major expressed TRPC4-associated protein (Figure. S4B). Regarding store-operated calcium entry (SOCE) components, Orai1, Orai2, and STIM1 were identified as the principal expressed proteins (Figure.S4C).

To identify hydrogen-dependent calcium channels, we conducted inhibitory and siRNA interference experiments targeting these identified channels. Pharmacological inhibition of T-type, L-type, or N-type VGCCs demonstrated minimal impact on $H_2$-enhanced calcium influx (Figure. S4D, Figure. S4E and Figure. S4F). Furthermore, $H_2$-mediated effects remained unaffected by TRPM4/7, TRPV2, Orai1/2, or STIM1 inhibition (Figure.S4 H, Figure.S4J, Figure.S4K, Figure.S4L, Figure.S4N, Figure.S4O, Figure.S4P, Figure.S4Q). Notably, both pan-TRPC family inhibitors (Figure.S4G) and specific TRPC4/5 antagonists (Figure.S4I) effectively abolished hydrogen-induced calcium influx.

The TRPC1, TRPC4, and TRPC5 channel proteins frequently assemble into heterotetrameric complexes, with TRPC4 exhibiting high homology to TRPC5. Gene

silencing experiments demonstrated that $H_2$-mediated $Ca^{2+}$ influx does not require TRPC5 or TRPC1 (Figure.S4I, Figure.S4L), but TRPC4 silencing markedly reduced $H_2$-induced effects (Fig. 4A, Fig. 4B). Importantly, $H_2$-triggered $Ca^{2+}$ influx remained unaffected by Giα knockdown, confirming its mechanism operates independently of Giα signaling (Figure. S4P).

Multichannel inhibition analyses identified TRPC4 and TRPC4AP as principal mediators of $H_2$-driven $Ca^{2+}$ influx (Fig. 4). Genetic ablation of TRPC4AP completely eliminated $H_2$-mediated regulation of $Ca^{2+}$ influx (Fig. 4C, Fig. 4D), establishing TRPC4AP as a crucial molecular target for $H_2$ action. TRPC4AP interacts directly with TRPC4 while maintaining associations with TRPC1 and TRPC5, implying its functional involvement in organizing heteromeric complexes among these proteins.

To delineate mechanistic contributions of TRPC4 and TRPC4AP in $H_2$ signaling, CRISPR-Cas9-generated TRPC4 and TRPC4AP knockout 293T cell lines were established (Fig.4E, Fig.4F), with sequencing data confirming knockout efficiency (Figure. S5). Both TRPC4 ($293T^{trpc4-}$) and TRPC4AP($293T^{trpc4ap-}$) cells exhibited complete loss of $H_2$-induced $Ca^{2+}$ responses (Fig.4G, Fig.4H, Fig.4K, Fig.4L). Functional restoration through reintroduction of wild-type TRPC4 (wt-trpc4) or TRPC4AP (wt-trpc4ap) reinstated calcium signaling responsiveness to $H_2$ in respective knockout models (Fig. 4I, Fig. 4J, Fig. 4M, Fig. 4N). These findings provide definitive evidence for the essential roles of TRPC4 and its interacting partner TRPC4AP in mediating $H_2$-dependent calcium signaling transduction pathways.

**Molecular Docking Prediction and Validation of the TRPC4-TRPC4AP Protein Binding Site**

To investigate the interaction between TRPC4 and TRPC4AP, we performed protein-protein docking analyses using the structural file of TRPC4 (PDB ID: 7b0j) and an AlphaFold-predicted model of TRPC4AP. From 2,000 potential docking conformations, we selected the top 60 TRPC4-TRPC4AP interaction patterns based on computational scoring metrics. Structural alignment revealed a unique cytokine-induced $SH_2$ domain-binding (CIRB) domain in TRPC4 (Fig. 5A, Fig. 5B), a critical regulatory element in cellular signaling. This domain typically facilitates interactions with $SH_2$ domains to coordinate essential cellular processes, including growth regulation, differentiation programming, migration control, and survival mechanisms.

Detailed analysis of TRPC4-TRPC4AP complex formation demonstrated that the CIRB domain of TRPC4 mediates interaction with TRPC4AP. Through amino acid frequency mapping of TRPC4 conserved regions (Fig. 5E, Fig. 5F) combined with computational modeling, we identified two adjacent arginine residues (positions 730 and 731) in the C-terminal region of the CIRB domain as primary interaction sites (Fig. 5C). Parallel predictive analyses using AlphaFold 3 and the same docking software revealed consistent binding patterns, with the interaction between TRPC4 arginine-730 and a glutamate residue on TRPC4AP achieving the highest protein scoring function (PSC) value (Fig. 5D). Both methodologies produced compatible spatial configurations and energetically favorable interaction profiles[27].

To elucidate the molecular basis of TRPC4-TRPC4AP interaction, we conducted systematic mutagenesis targeting arginine residues at positions 730 and 731 within the

CIRB motif. AlphaFold 3-based structural predictions demonstrated complete disruption of protein-protein interaction upon single (R730A) or double (R730A/R731A) mutations (Fig. 5G, Fig. 5H), establishing the essential role of these conserved residues in complex formation.

To verify the predictions made by molecular docking, we constructed amino acid mutation vectors in the px459 system, guided by human amino acid preferences. We mutated the wild-type arginines (wt$730^{Arg}731^{Arg}$) in the CIRB motif to $730^{Ala}731^{Arg}$ and $730^{Ala}730^{Ala}$ to investigate the dependence of $H_2$ on the TRPC4-TRPC4AP binding site. The results demonstrated that, in the presence of $H_2$, $Ca^{2+}$ concentration in the px459 pressure screening control group increased more than twofold (Fig. 5I, Fig. 5J), while the *trpc4*KO cell line showed no response to $H_2$-induced $Ca^{2+}$ influx (Fig. 5K, Fig. 5L). Upon complementing the *trpc4*KO cell line with px459-$730^{Ala}730^{Ala}$ (Fig. 5M, Fig. 5N) and px459-$730^{Ala}731^{Arg}$ (Fig. 5O, Fig. 5P), the $H_2$-mediated promotion of $Ca^{2+}$ influx was lost. These findings confirm that $H_2$ relies on TRPC4AP to enhance cellular $Ca^{2+}$ influx and that the binding site comprising $730^{Arg}731^{Arg}$ on TRPC4-TRPC4AP at the CIRB motif is crucial for the opening of the $Ca^{2+}$ channel.

**$H_2$ enhanced cell motility by inducing $Ca^{2+}$ influx to reconstruct cytoskeleton**

Immunofluorescence (IF) analysis revealed predominant cytoplasmic localization of TRPC4AP in mesenchymal stem cells (MSCs) with no colocalization observed with the F-actin cytoskeletal network (Fig. 6A). Live-cell imaging over a 3-hour period demonstrated significantly accelerated F-actin cytoskeletal contraction dynamics in $H_2$-treated MSCs compared to untreated controls (Fig. 6B), indicative of enhanced cellular motility. Protein expression profiling showed coordinated upregulation of mesenchymal markers, with vimentin and α-smooth muscle actin (α-SMA) levels increasing post-$H_2$ treatment across multiple MSC subtypes (Fig. 6C, Fig. 6D). Ultrastructural analysis via transmission electron microscopy (TEM) revealed characteristic membrane-proximal aggregation of microfilament bundles following both acute (2-hour) and prolonged (24-hour) $H_2$ exposure (Fig. 6E).

Functional assessments through scratch wound assays demonstrated significant $H_2$-mediated migration enhancement, with wound closure rates reaching 58% in treated groups versus 38% in controls at 24 hours. This pro-motility effect was substantially attenuated by trpc4ap knockdown, confirming pathway specificity. While histamine (a calcium agonist positive control) induced moderate calcium influx (Figure.S6A, Figure.S6B) and upregulated vimentin (Figure.S6C), α-SMA (Figure.S6D), and collagen I (Figure.S6D) expression, its efficacy remained inferior to $H_2$ stimulation.

Mechanistic investigation through time-course transcriptomics identified seven consensus differentially expressed genes (DEGs) common to both 2-hour and 24-hour $H_2$ treatments (Fig. 6G, Fig. 6H). Gene set enrichment analysis (GSEA) revealed significant calcium channel-related pathway activation at both time points (Fig.6I, Fig. 6J), corroborating the functional data.

These integrated findings establish that $H_2$-induced extracellular calcium influx primarily orchestrates cytoskeletal reorganization and motility enhancement in MSCs through TRPC4AP-dependent mechanisms.

RNA-seq analysis revealed that individual clustering showed upregulated genes in the

MSCs-2h-$H_2$ group were primarily enriched in extracellular matrix (ECM) organization and tubule development (Figure. S7A), indicating significant modulations in the cytoskeleton. In the MSCs-24h-$H_2$ group, upregulated genes were mainly associated with muscle movement and $Ca^{2+}$ transport (Figure. S7B), suggesting enhanced cell motility. Joint clustering analysis indicated that upregulated genes in the MSCs-2h-$H_2$ group were predominantly linked to fat cell, epithelium, and muscle cell differentiation, as well as muscle cell proliferation (Fig. 6K).

The effect of $H_2$ was validated in the HUVEC cell line, demonstrating that $H_2$ similarly enhances the migratory capabilities of cells, evidenced by accelerated wound healing speed (Figure. S8A) and rapid reorganization of the cytoskeleton (Figure. S8B). Transcriptomic analysis conducted 2 hours post $H_2$ treatment (2h-$H_2$ vs 2h-Ctrl) revealed significant inter-group differences, with an increased number of DEGs (Figure. S8C-S8E). GO and KEGG enrichment analyses indicated upregulation of processes related to development and ion regulation, along with cytoskeletal gene enrichment and notable activation of the calcium signaling pathway (Figure. S8F). This suggests that $H_2$ may modulate cytoskeletal remodeling in HUVECs through transient $Ca^{2+}$ influx. By 24 hours, the upregulated genes were primarily associated with cytokine signaling, while genes related to $Ca^{2+}$ influx were downregulated (Figure. S8F), indicating a shift towards $Ca^{2+}$ efflux or cessation of influx, thereby initiating downstream signaling cascades.

**$H_2$ Effects on Intracellular Cations**

The TRP channel is a non-selective cation channel composed of four subunits, which is permeable to a variety of cations, including $Ca^{2+}$, $K^+$, and $Na^+$( Figure. S3 ). These cations exhibit competitive interactions within the channel, with $Ca^{2+}$ generally being more permeable than $Na^+$ and $K^+$. In this study, we used $Na^+$/$K^+$ ion probes to investigate the ion influx in MSCs (Figure. S3A). We found that after adding $H_2$ to the regular culture medium, there was a slight increase in $Na^+$ levels in the cytoplasm, while $K^+$ influx remained unchanged. When the medium was switched to a Ca2+-free solution, $Na^+$ influx continued to rise, while $K^+$ influx still showed no significant change. These results suggest that hydrogen gas induces cation influx through TRPC4, where $Ca^{2+}$ exhibits a much higher permeability than $Na^+$ and $K^+$. The slight increase in $Na^+$ may be related to the NAX system, which helps expel excess $Ca^{2+}$ that enters the cell. A similar phenomenon was observed in HUVECs (Figure. S3B).

**Discussion**

$Ca^{2+}$, as ubiquitous secondary messengers, orchestrate critical biological processes in eukaryotic cells, including gene expression, metabolic homeostasis, cell cycle progression, cellular motility, and neuromuscular signaling[1, 12, 28]. This study reveals that $H_2$ specifically activates the TRPC4-TRPC4AP signaling axis to induce calcium influx, uncovering for the first time the molecular mechanism by which $H_2$ functions as a novel calcium signaling agonist. To elucidate the molecular targets of $H_2$, we integrated computational structural biology with functional validation experiments: Molecular docking simulations identified a dual-arginine motif (730Arg-731Arg) within the carboxyl-terminal CIRB domain of TRPC4 as the $H_2$-binding pocket. Subsequent site-directed mutagenesis confirmed that this motif serves as a critical regulatory site for calcium channel activation in the TRPC4AP-TRPC4 complex. Molecular dynamics simulations further suggested that

$H_2$ enhances the conformational stability of the ion channel by restructuring the hydrogen-bonding network of arginine residues and modulating local electrostatic potential. These findings not only establish a novel paradigm for gasotransmitter-mediated calcium homeostasis regulation but also provide an innovative structural framework for targeted drug design toward TRPC4 channels.

**Hydrogen Gas: Broad-Spectrum Effects and Calcium Homeostasis Regulation**

According to the Human Protein Atlas[29], the TRPC4AP gene and its encoded protein are ubiquitously expressed across diverse tissue types (Figure. S9A, Figure. S9C). Although proteomic data for TRPC4 remain limited, transcriptomic profiling reveals tissue-specific enrichment of TRPC4 mRNA in the endometrium, seminal vesicles, and smooth muscle tissues (Figure. S9B, Figure. S9D). Strikingly, $H_2$-induced $Ca^{2+}$ influx demonstrates broad-spectrum functionality, as evidenced by extracellular calcium entry triggered by hydrogen in mesenchymal stem cells, endothelial cells, epithelial cells, fibroblasts, osteoblasts, and cardiomyocytes (Fig.1A, Fig. 2A-F, Fig. 3J). Furthermore, in vivo experiments substantiate this universality: hydrogen exposure significantly amplifies $Ca^{2+}$ transients in mouse primary motor cortex (M1) neurons (Fig. 2G-J), indicating $H_2$ enhances neuronal $Ca^{2+}$ concentrations to potentiate synaptic transmission. These findings collectively validate the pan-cellular nature of $H_2$-mediated calcium signaling across both in vitro and in vivo systems.

Cellular viability critically depends on maintaining cytosolic $Ca^{2+}$ within a narrow physiological range (~200 nM in quiescent cells)[30]. Dysregulated calcium accumulation or depletion triggers pathological cascades leading to cellular senescence or apoptosis. This equilibrium is governed by a multi-tiered regulatory network: (1) PMCA (plasma membrane $Ca^{2+}$-ATPase) and NCX (sodium-calcium exchanger)-mediated $Ca^{2+}$ extrusion[17, 31]; (2) ER/SR calcium buffering and storage; (3) coordinated gating of plasma membrane calcium channels[32]. Our data reveal that $H_2$-induced $Ca^{2+}$ elevation exhibits spatiotemporal compartmentalization: early-phase $Ca^{2+}$ influx via TRPC4 channels is partially sequestered into the ER (Fig. 2G, Fig. 2H), while later-phase $Ca^{2+}$ efflux occurs predominantly through NCX transporters (Fig.3J-L).

Notably, acute $H_2$ treatment elicits dual beneficial effects: (1) Cell viability remains uncompromised (Fig. 3A, Fig. 3G) with preserved mitochondrial integrity (Fig.3B-D)[33], confirming absence of cytotoxicity; (2) Further measurement of Ca-Mg-ATPase activity at different time points revealed that the enzyme activity in the $H_2$ group increased over time, showing a gradually rising trend (Fig.3L), and reached more than six times that of the control group after 30 minutes. (3) Another channel for calcium extrusion at the cell membrane is NXC, and since the $Na^+$ concentration did not change significantly (Figure S3B, D), the role of this channel in calcium extrusion is excluded.

**$H_2$-mediated $Ca^{2+}$ influx originates extracellularly and depends on TRPC4 channel activity**

TRPC ion channels constitute a class of non-selective cation channels that play a pivotal role in regulating a wide range of cellular functions, including nociception[34], mechanosensation[35], and signal transduction processes[36]. TRPC4 is broadly expressed across human tissues, with the Human Atlas Database identifying its presence in multiple organs, such as the heart, vasculature, brain, lungs, and kidneys (Figure.S9A,

Figure.S9D). Functionally, TRPC4 can assemble as a homotetrameric channel or form heterotetrameric complexes with TRPC1 and TRPC5[32, 37]. Among these three subunits, TRPC4 and TRPC5 exhibit a higher degree of sequence homology. Accumulating research evidence suggests that TRPC1 functions as a negative regulator of TRPC4 and TRPC5, thereby modulating their physiological roles[38].

Through the use of calcium-free culture media replacement, pharmacological calcium depletion, and calcium ion tracing in both the mitochondria and endoplasmic reticulum[39], we determined that hydrogen-induced calcium influx primarily originates from extracellular sources (Fig. 1G, Fig. 1H), with minimal contributions from intracellular calcium stores, including the ER (Fig. 1K) and Mito (Fig 1L). Given these findings, we directed our focus towards $Ca^{2+}$ channels located on the plasma membrane. Transcriptomic sequencing enabled us to quantify the expression levels of all proteins associated with calcium ion channels (Figure.S4A–S4C). Subsequent inhibitor studies and siRNA knockdown experiments further refined our focus to TRPC1, TRPC4, and TRPC5 as the key channels involved in this process.

Following the knockdown of TRPC1 and TRPC5, we observed that $H_2$ remained capable of inducing $Ca^{2+}$ influx. However, while knockdown of TRPC1 resulted in a moderate attenuation of $H_2$-induced effects, silencing TRPC4 led to a significant reduction in $Ca^{2+}$ influx. Additionally, transcriptomic sequencing revealed that among the TRPC family members, TRPC1 and TRPC4 exhibited higher baseline gene expression levels (Figure S4B), suggesting that TRPC1 may play a role in the assembly of the TRPC4 channel complex. Liu et al. demonstrated that TRPC4 is expressed in cerebral vasculature, where it is regulated by GPCRs and receptor tyrosine kinases, thereby facilitating $Ca^{2+}$ influx and modulating vasodilation[40]. However, the effects of $H_2$ appear to be independent of Giα signaling (Figure. S4P) and may instead be mediated through TRPC4AP, which regulates the opening of TRPC4.

**TRPC4AP: A Molecular Switch for Hydrogen-Induced Activation of the TRPC4 Calcium Channel**

TRPC4AP can directly bind to TRPC4 and interact with TRPC1, TRPC4, and TRPC5[26, 41]. To date, only the TRPC4-TRPC4AP complex has been demonstrated to trigger calcium loading upon depletion of ER $Ca^{2+}$ stores, suggesting that this pathway may regulate $Ca^{2+}$ influx[26]. Transcriptomic sequencing revealed that among TRPC-related genes, trpc4ap exhibited the highest baseline expression level (Figure S4B). Moreover, the effect of $H_2$ on $Ca^{2+}$ influx was entirely dependent on TRPC4AP (Fig.4C, Fig.4D, Fig.4G, Fig.4H, Fig.4I, Fig.4J). Similarly, the influence of $H_2$ on cellular functions, including cytoskeletal dynamics (Figure 6B, E), migration (Fig. 6F), and differentiation (Fig.6C, Fig.6D), was strictly dependent on TRPC4AP expression. Furthermore, the effect of $H_2$ on $Ca^{2+}$ influx was nearly abolished in TRPC4-deficient cells (Fig.4A, Fig.4B, Fig.4K, Fig.4L). These findings suggest that $H_2$ primarily relies on the molecular switch function of TRPC4AP to activate TRPC4 channels and facilitate $Ca^{2+}$ influx.

**Elucidating the TRPC4-TRPC4AP Molecular Interaction Interface: Identification of Hydrogen ($H_2$)-Sensitive Functional Domains**

The interaction between TRPC4 and TRPC4AP is currently unknown, with scant structural evidence available[42]. The IF staining indicates that TRPC4AP, resembling a

scaffolding structure, is abundantly expressed throughout the cytoplasm (Fig. 6A). While the specific binding sites between TRPC4AP and TRP proteins remain unidentified. To address this, we performed molecular docking simulations between TRPC4 and TRPC4AP, which may relate to $H_2$, predicting key binding sites at 730Arg and 731Arg on TRPC4 (Fig. 5E-5H). This binding site is located within the C-terminal CIRB functional box of TRPC4[43], a domain known to act as a switch for TRPC channels and previously identified as a binding site for IP3Rs, which regulate the endogenous SOCE, and calmodulin (CaM)[43], an inhibitor of IP3R, which binds to the CIRB box and activates TRPC4[44, 45] . The CIRB box is specifically present inTRPC4 subtypes and absent/different in TRPC1 and TRPC5, as shown by sequence alignment (Fig. 5A, Fig. 5B). This specificity suggests the unique role of this TRPC4 binding site within heterotetrameric complexes.

The predicted binding sites for TRPC4-TRPC4AP interaction, including ionic and hydrogen bond interactions, are primarily located within the basic amino acid-rich region of the C-terminal of TRPC4. Analysis of the frequency of amino acid occurrences in the 60 selected binding poses reveals that Arg and Lys are the most frequently represented amino acids. Notably, 730Arg and 731Arg in the CIRB-box, which appear as consecutive basic amino acids, show the highest frequency and are key sites critical to $H_2$ function (Fig. 5C). Single and double amino acid mutations at the 730Arg and 730Arg/731Arg site and subsequent complementation indicated a critical dependency of $H_2$ on the TRPC4-TRPC4AP binding site (Fig.7A). Additionally, Lys is found frequently, appearing 80 times in the 60 binding poses (Fig. 4F). This suggests that 715Lys and 716Lys, located in the Protein 4.1 module upstream of the CIRB motif, may also be potential sites affected by $H_2$. Other possible sites include 737Arg and 738Arg within the CIRB, as well as 718Arg and 719Arg in the Protein 4.1 module (Fig.5B), all of which warrant further validation and investigation.

The binding sites likely influenced by $H_2$ are predominantly basic amino acids. In the exploratory extension of this study, NMT analysis indicates that $H_2$ exposure leads to proton extrusion (Fig. 7B, Fig. 7C), while pH fluorescent probes suggest an increase in intracellular pH (Fig.7D, Fig.7E), creating an alkaline microenvironment[46, 47]. Such conditions are favorable for the stability of basic amino acids. These observations imply that $H_2$ may indirectly modulate TRPC4-TRPC4AP binding by altering the intracellular acid-base environment. Previous studies have shown that eukaryotic plant plasma membranes possess hydrogenase activity, capable of decomposing and utilizing molecular $H_2$, which in turn promotes proton extrusion and accelerates hypocotyl growth in mung beans , aligning with our findings. While hydrogenase activity has not yet been identified in animal cell membranes, our data suggest that $H_2$ could alter protein interaction sites on the cell membrane by modulating local acidity or alkalinity. This points to a potential metabolic role for $H_2$ at the cell membrane (Fig.7F), which requires further exploration.

**$H_2$ May Regulate Multiple Biological Functions Through the Multifunctional Docking Site of TRPC4AP**

In addition to its interaction with TRPC1/4/5, TRPC4AP exhibits multiple functions[48]. It has been identified as a key substrate-recognition component of the DCX

(DDB1-CUL4-X-box) E3 ubiquitin-protein ligase complex, which is crucial for regulating the cell cycle[49, 50] . Further investigations have revealed that the DCX (TRPC4AP) complex specifically mediates the polyubiquitination and subsequent degradation of MYC via the DesCEND (destruction via C-end degrons) pathway[50]. This mechanism also helps explain the typically lower expression levels of TRPC4AP observed in tumor cell lines compared to normal cells, resulting in distinct responses to $H_2$, as shown in Figure .S10.

TRPC4AP, also known as TNF-R1 ubiquitous scaffolding and signaling protein, plays a pivotal role in the activation of NFκB1 upon TNFRSF1A ligation, potentially by bridging TNFRSF1A to the IKK signaling pathway[51]. Furthermore, TRPC4AP is instrumental in activating both NF-κB and c-Jun N-terminal kinase (JNK) in response to TNF-α stimulation[52] . This multifaceted involvement highlights the essential role of TRPC4AP in the complex signaling networks that regulate cellular responses to TNF-α, demonstrating its importance in the orchestration of inflammatory and immune signaling pathways[53].

The multifaceted roles of TRPC4AP exhibit notable parallels with the functions of $H_2$, particularly its ability to mitigate inflammatory storm responses and reduce inflammation-induced tissue damage[24, 54, 55]. Additionally, $H_2$ has been shown to promote cellular proliferation and activation in various cell types, including epidermal stem cells, fibroblasts, and epithelial cells . Given that TRPC4AP is considered a key protein dependent on $H_2$ for its function in facilitating $Ca^{2+}$ influx, it is highly plausible that the diverse biological effects of $H_2$ are linked to the ubiquitination and inflammation-related signaling pathways associated with TRPC4AP. This suggests that TRPC4AP may play a critical role in mediating the pleiotropic effects of $H_2$ in cellular processes, particularly those involving inflammation and cellular activation.

**Therapeutic Implications and Future Directions**

Endogenous $H_2$, predominantly produced by gut microbiota with a daily yield of 0.2-1.5 liters, serves as a critical modulator of metabolic processes[56, 57]. Within the intestinal ecosystem, $H_2$ exhibits dual functionality—participating in both its own biosynthesis and catabolism—thereby regulating secondary metabolite conversion. We propose that interindividual variations in gut microbiota composition drive heterogeneous $H_2$ levels, which may differentially influence $Ca^{2+}$ flux dynamics and downstream physiological outcomes.

Excessive $Ca^{2+}$ influx acts as a pathogenic driver across multiple cellular processes: Neurodegeneration: Mitochondrial calcium signaling disruption correlates with Alzheimer's[58], Parkinson's[59], and Huntington's pathologies[60]. Immune Dysfunction: Calcium signaling pathways are indispensable for lymphocyte activation and immune disorder progression. While $H_2$ demonstrates unique calcium-modulating capacity, its therapeutic application requires stringent optimization of: dosage thresholds and temporal dynamics.

Our discovery of the $H_2$-TRPC4/TRPC4AP regulatory axis unveils a groundbreaking therapeutic approach for calcium homeostasis disorders. This molecular switch enables:

(1) precision-targeted correction of calcium overload while preserving physiological fluctuations, (2) tissue-selective modulation of calcium-dependent signaling cascades, and (3) prevention of compensatory stress responses typically associated with conventional calcium channel blockers. These findings are anticipated to systematically elucidate the multifaceted physiological roles of $H_2$ in critical biological processes.

## Conclusion

This study elucidates the molecular mechanism by which $H_2$ functions as a first-in-class calcium signaling agonist, demonstrating its capacity to modulate calcium dynamics through the TRPC4-TRPC4AP channel axis. Our findings reveal that $H_2$ binds to a discrete arginine-rich motif (730Arg-731Arg) within the CIRB domain of TRPC4, triggering conformational changes that potentiate extracellular $Ca^{2+}$ influx while maintaining calcium homeostasis. This gasotransmitter-like activity establishes $H_2$ as a unique endogenous regulator of calcium signaling networks.

## Disclosure and competing interest statement

The authors declare no conflict of interest.

## Author Contributions

Conceptualization P.Z. and X.M.; Data curation, P.Z., H.L., and Z.C.; Formal analysis, X.Z., X.W., Z.L., and S.J.; Funding acquisition, X.M. and P.Z.; Methodology, Z.C., P.Z., H.L., X.Z., Z.D., X.J., and J.W.; Visualization, P.Z., H.L., Z.C., and X.Z.; Writing – original draft, P.Z.; Writing – review & editing, X.Z., M.L., F.X. and X.M. All authors have read and agreed to the published version of the manuscript.

## Data availability statement

The original contributions presented in this study are included in the article/Supplementary.

## Acknowledgments

We thank Biorender (www.biorender.com) for their drawing assistance during the writing of this article.

## Ethics statement

The study was conducted in accordance with the Declaration of Helsinki.

## Funding

This research was funded Military Logistics Key Open Research Projects (China BHJ17L018); sponsored by Beijing Nova Program (20220484218).

## References


1. Clapham DE: **Calcium signaling**. *Cell* 2007, **131**(6):1047-1058.

2. Zheng J, Zeng X, Wang S: **Calcium ion as cellular messenger**. In., vol. 58: Springer; 2015: 1-5.

3. Ghosh A, Ginty DD, Bading H, Greenberg ME: **Calcium regulation of gene expression**

**in neuronal cells**. *Journal of neurobiology* 1994, **25**(3):294-303.

4. Kahl CR, Means AR: **Regulation of cell cycle progression by calcium/calmodulin-dependent pathways**. *Endocrine reviews* 2003, **24**(6):719-736.

5. Zheng JQ, Poo M-m: **Calcium signaling in neuronal motility**. *Annu Rev Cell Dev Biol* 2007, **23**(1):375-404.

6. Kondratskyi A, Kondratska K, Skryma R, Klionsky DJ, Prevarskaya N: **Ion channels in the regulation of autophagy**. *Autophagy* 2018, **14**(1):3-21.

7. Honda H, Kondo T, Zhao Q-L, Feril Jr LB, Kitagawa H: **Role of intracellular calcium ions and reactive oxygen species in apoptosis induced by ultrasound**. *Ultrasound in medicine & biology* 2004, **30**(5):683-692.

8. Dolphin AC, Lee A: **Presynaptic calcium channels: specialized control of synaptic neurotransmitter release**. *Nature Reviews Neuroscience* 2020, **21**(4):213-229.

9. Li HF, Li XY, Sun YQ, Zhi ZY, Song LF, Li M, Feng YM, Zhang ZH, Liu YF, Chen YJ: **The Role of Ion Channels in Pulmonary Hypertension: A Review**. *Pulmonary Circulation* 2025, **15**(1):e70050.

10. Suzuki K: **Thrombomodulin: A key regulator of intravascular blood coagulation, fibrinolysis, and inflammation, and a treatment for disseminated intravascular coagulation**. *Proceedings of the Japan Academy, Series B* 2025, **101**(2):75-97.

11. Makiyama F, Kawase S, Omi AW, Tanikawa Y, Kotani T, Shirayama T, Nishimura N, Kurihara T, Saito N, Takahashi J: **Differential effects of structurally different lysophosphatidylethanolamine species on proliferation and differentiation in pre-osteoblast MC3T3-E1 cells**. *Scientific Reports* 2025, **15**(1):466.

12. Berridge MJ, Bootman MD, Roderick HL: **Calcium signalling: dynamics, homeostasis and remodelling**. *Nature reviews Molecular cell biology* 2003, **4**(7):517-529.

13. Cartes-Saavedra B, Ghosh A, Hajnóczky G: **The roles of mitochondria in global and local intracellular calcium signalling**. *Nature Reviews Molecular Cell Biology* 2025:1-20.

14. Rizzuto R, Pinton P, Carrington W, Fay FS, Fogarty KE, Lifshitz LM, Tuft RA, Pozzan T: **Close contacts with the endoplasmic reticulum as determinants of mitochondrial $Ca^{2+}$ responses**. *Science* 1998, **280**(5370):1763-1766.

15. Hoth M, Fanger CM, Lewis RS: **Mitochondrial regulation of store-operated calcium signaling in T lymphocytes**. *The Journal of cell biology* 1997, **137**(3):633-648.

16. Suzuki J, Kanemaru K, Ishii K, Ohkura M, Okubo Y, Iino M: **Imaging intraorganellar $Ca^{2+}$ at subcellular resolution using CEPIA**. *Nature communications* 2014, **5**(1):4153.

17. Raffaello A, Mammucari C, Gherardi G, Rizzuto R: **Calcium at the center of cell signaling: interplay between endoplasmic reticulum, mitochondria, and lysosomes**. *Trends in biochemical sciences* 2016, **41**(12):1035-1049.

18. Emrich SM, Yoast RE, Trebak M: **Physiological functions of CRAC channels**. *Annual Review of Physiology* 2022, **84**(1):355-379.

19. Nilius B, Owsianik G: **The transient receptor potential family of ion channels**. *Genome biology* 2011, **12**:1-11.

20. Bacsa B, Tiapko O, Stockner T, Groschner K: **Mechanisms and significance of $Ca^{2+}$ entry through TRPC channels**. *Current opinion in physiology* 2020, **17**:25-33.

21. Zhang M, Ma Y, Ye X, Zhang N, Pan L, Wang B: **TRP (transient receptor potential) ion**

**channel family: structures, biological functions and therapeutic interventions for diseases**. *Signal Transduction and Targeted Therapy* 2023, **8**(1):261.

22. Bechem M, Schramm M: **Calcium-agonists**. *Journal of molecular and cellular cardiology* 1987, **19**:63-75.

23. Tarr TB, Malick W, Liang M, Valdomir G, Frasso M, Lacomis D, Reddel SW, Garcia-Ocano A, Wipf P, Meriney SD: **Evaluation of a novel calcium channel agonist for therapeutic potential in Lambert–Eaton myasthenic syndrome**. *Journal of Neuroscience* 2013, **33**(25):10559-10567.

24. Ohta S: **Molecular hydrogen as a preventive and therapeutic medical gas: initiation, development and potential of hydrogen medicine**. *Pharmacology & therapeutics* 2014, **144**(1):1-11.

25. Ohsawa I, Ishikawa M, Takahashi K, Watanabe M, Nishimaki K, Yamagata K, Katsura K-i, Katayama Y, Asoh S, Ohta S: **Hydrogen acts as a therapeutic antioxidant by selectively reducing cytotoxic oxygen radicals**. *Nature medicine* 2007, **13**(6):688-694.

26. Mace KE, Lussier MP, Boulay G, Terry-Powers JL, Parfrey H, Perraud AL, Riches DW: **TRUSS, TNF-R1, and TRPC ion channels synergistically reverse endoplasmic reticulum $Ca^{2+}$ storage reduction in response to m1 muscarinic acetylcholine receptor signaling**. *Journal of cellular physiology* 2010, **225**(2):444-453.

27. Abramson J, Adler J, Dunger J, Evans R, Green T, Pritzel A, Ronneberger O, Willmore L, Ballard AJ, Bambrick J: **Accurate structure prediction of biomolecular interactions with AlphaFold 3**. *Nature* 2024, **630**(8016):493-500.

28. Staruschenko A, Alexander RT, Caplan MJ, Ilatovskaya DV: **Calcium signalling and**

**transport in the kidney**. *Nature Reviews Nephrology* 2024, **20**(8):541-555.

29. Pontén F, Jirström K, Uhlen M: **The Human Protein Atlas—a tool for pathology**. *The Journal of Pathology: A Journal of the Pathological Society of Great Britain and Ireland* 2008, **216**(4):387-393.

30. Peacock M: **Calcium metabolism in health and disease**. *Clinical Journal of the American society of nephrology* 2010, **5**(Supplement_1):S23-S30.

31. Di Leva F, Domi T, Fedrizzi L, Lim D, Carafoli E: **The plasma membrane $Ca^{2+}$ ATPase of animal cells: structure, function and regulation**. *Archives of biochemistry and biophysics* 2008, **476**(1):65-74.

32. Brini M, Calì T, Ottolini D, Carafoli E: **The plasma membrane calcium pump in health and disease**. *The FEBS journal* 2013, **280**(21):5385-5397.

33. Zhao P, Dang Z, Liu M, Guo D, Luo R, Zhang M, Xie F, Zhang X, Wang Y, Pan S: **Molecular hydrogen promotes wound healing by inducing early epidermal stem cell proliferation and extracellular matrix deposition**. *Inflammation and Regeneration* 2023, **43**(1):22.

34. Sun Z-C, Ma S-B, Chu W-G, Jia D, Luo C: **Canonical transient receptor potential (TRPC) channels in nociception and pathological pain**. *Neural Plasticity* 2020, **2020**(1):3764193.

35. Eijkelkamp N, Quick K, Wood JN: **Transient receptor potential channels and mechanosensation**. *Annual review of neuroscience* 2013, **36**(1):519-546.

36. Pedersen SF, Owsianik G, Nilius B: **TRP channels: an overview**. *Cell calcium* 2005, **38**(3-4):233-252.

37. Duan J, Li J, Zeng B, Chen G-L, Peng X, Zhang Y, Wang J, Clapham DE, Li Z, Zhang J: **Structure of the mouse TRPC4 ion channel**. *Nature Communications* 2018, **9**(1):3102.

38. Kim J, Ko J, Myeong J, Kwak M, Hong C, So I: **TRPC1 as a negative regulator for TRPC4 and TRPC5 channels**. *Pflügers Archiv-European Journal of Physiology* 2019, **471**:1045-1053.

39. Malli R, Frieden M, Trenker M, Graier WF: **The role of mitochondria for Ca2+ refilling of the endoplasmic reticulum**. *Journal of Biological Chemistry* 2005, **280**(13):12114-12122.

40. Liu D, Xiong S, Zhu Z: **Imbalance and dysfunction of transient receptor potential channels contribute to the pathogenesis of hypertension**. *Science China Life Sciences* 2014, **57**:818-825.

41. Mace KE: **Intersecton of cellular signaling cascades with TRPC ion channel responses and calcium ion homeostasis**. University of Colorado Health Sciences Center; 2009.

42. Poduslo SE, Huang R, Huang J, Smith S: **Genome screen of late-onset Alzheimer's extended pedigrees identifies TRPC4AP by haplotype analysis**. *American Journal of Medical Genetics Part B: Neuropsychiatric Genetics* 2009, **150**(1):50-55.

43. Zhu MX: **Multiple roles of calmodulin and other Ca 2+-binding proteins in the functional regulation of TRP channels**. *Pflügers Archiv* 2005, **451**:105-115.

44. Freichel M, Tsvilovskyy V, Camacho-Londoño JE: **TRPC4-and TRPC4-containing channels**. *Mammalian Transient Receptor Potential (TRP) Cation Channels: Volume I* 2014:85-128.

45. Vinayagam D, Quentin D, Yu-Strzelczyk J, Sitsel O, Merino F, Stabrin M, Hofnagel O, Yu M, Ledeboer MW, Nagel G: **Structural basis of TRPC4 regulation by calmodulin and pharmacological agents**. *Elife* 2020, **9**:e60603.

46. Zhang X, Xie F, Zhang Z, Adzavon YM, Su Z, Zhao Q, LeBaron TW, Li Q, Lyu B, Liu G: **Hydrogen evolution and absorption phenomena in the plasma membrane of Vigna radiata and Capsicum annuum**. *Journal of Plant Growth Regulation* 2023, **42**(1):249-259.

47. Han M, Yang H, Yu G, Jiang P, You S, Zhang L, Lin H, Liu J, Shu Y: **Application of Non-invasive Micro-test Technology (NMT) in environmental fields: A comprehensive review**. *Ecotoxicology and Environmental Safety* 2022, **240**:113706.

48. Zeng C, Tian F, Xiao B: **TRPC channels: prominent candidates of underlying mechanism in neuropsychiatric diseases**. *Molecular neurobiology* 2016, **53**(1):631-647.

49. Choi SH, Wright JB, Gerber SA, Cole MD: **Myc protein is stabilized by suppression of a novel E3 ligase complex in cancer cells**. *Genes & development* 2010, **24**(12):1236-1241.

50. Koren I, Timms RT, Kula T, Xu Q, Li MZ, Elledge SJ: **The eukaryotic proteome is shaped by E3 ubiquitin ligases targeting C-terminal degrons**. *Cell* 2018, **173**(7):1622-1635. e1614.

51. Terry Powers JL, Mace KE, Parfrey H, Lee S-J, Zhang G, Riches DW: **TNF receptor-1 (TNF-R1) ubiquitous scaffolding and signaling protein interacts with TNF-R1 and TRAF2 via an N-terminal docking interface**. *Biochemistry* 2010, **49**(36):7821-7829.

52. Soond SM, Terry JL, Colbert JD, Riches DW: **TRUSS, a novel tumor necrosis factor receptor 1 scaffolding protein that mediates activation of the transcription factor NF-κB**. *Molecular and cellular biology* 2003, **23**(22):8334-8344.

53. Soond SM, Terry JL, Riches DW: **TRUSS, a tumor necrosis factor receptor-1-interacting protein, activates c-Jun $NH_2$-terminal kinase and transcription factor AP-1**. *FEBS letters* 2006, **580**(19):4591-4596.

54. Tian Y, Zhang Y, Wang Y, Chen Y, Fan W, Zhou J, Qiao J, Wei Y: **Hydrogen, a novel therapeutic molecule, regulates oxidative stress, inflammation, and apoptosis**. *Frontiers in physiology* 2021, **12**:789507.

55. Yang M, Dong Y, He Q, Zhu P, Zhuang Q, Shen J, Zhang X, Zhao M: **Hydrogen: a novel option in human disease treatment**. *Oxidative Medicine and Cellular Longevity* 2020, **2020**(1):8384742.

56. Zhang Y, Xu J, Yang H: **Hydrogen: An endogenous regulator of liver homeostasis**. *Frontiers in Pharmacology* 2020, **11**:877.

57. Tadross MR, Dick IE, Yue DT: **Mechanism of local and global $Ca^{2+}$ sensing by calmodulin in complex with a $Ca^{2+}$ channel**. *Cell* 2008, **133**(7):1228-1240.

58. Rahman MH, Bajgai J, Fadriquela A, Sharma S, Trinh Thi T, Akter R, Goh SH, Kim C-S, Lee K-J: **Redox effects of molecular hydrogen and its therapeutic efficacy in the treatment of neurodegenerative diseases**. *Processes* 2021, **9**(2):308.

59. Ostojic SM: **Inadequate production of $H_2$ by gut microbiota and Parkinson disease**. *Trends in Endocrinology & Metabolism* 2018, **29**(5):286-288.

60. Paul BD: **Cysteine metabolism and hydrogen sulfide signaling in Huntington's disease**.

*Free Radical Biology and Medicine* 2022, **186**:93-98.

**Figure titles and legends**

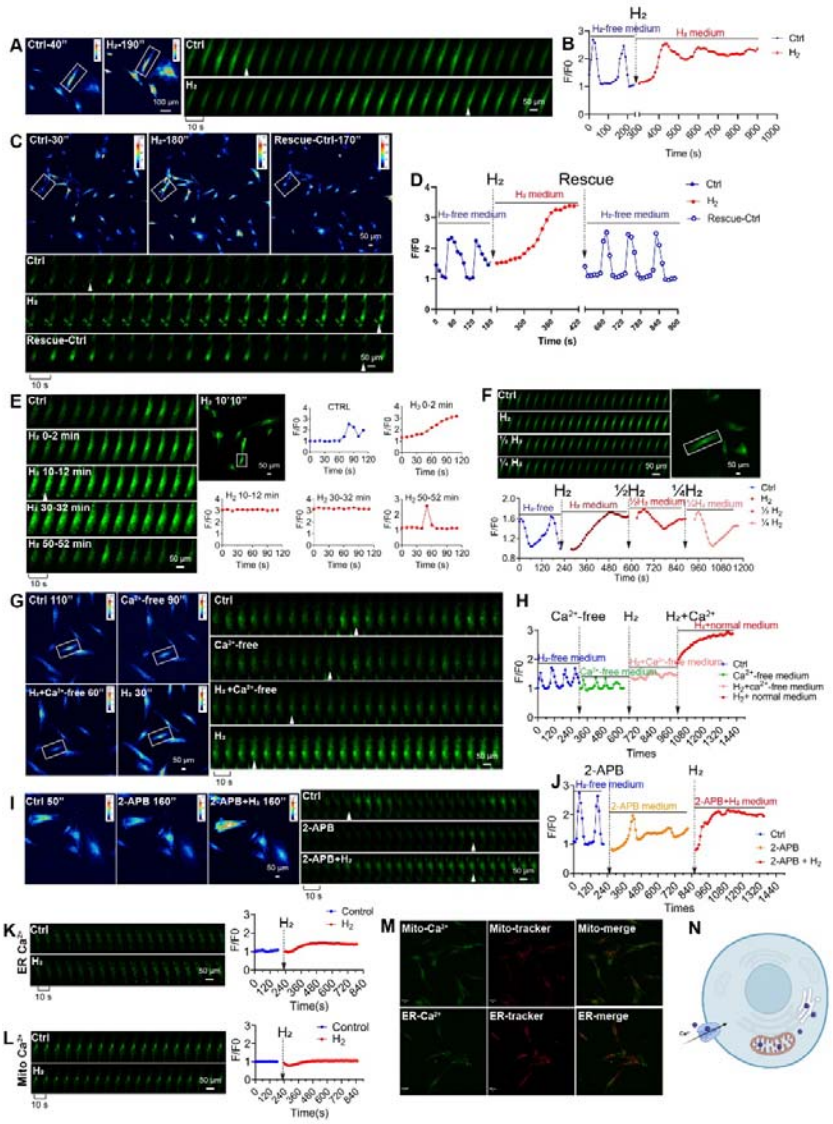

**Fig. 1. Dynamic time-lapse $Ca^{2+}$ imaging by the Stimulation of molecular $H_2$ induces $[Ca^{2+}]i$ oscillations in MSCs.** A. Pseudocolor and time series images of the $[Ca^{2+}]i$ changes under $H_2$-free and $H_2$-medium conditions. B. Fluo 4 averaged F/F0 trace in imaging $H_2$-free (blue) and $H_2$-medium conditions (red). C & D, Pseudocolor (C left, upper) and time series (C left, lower) images and the Fluo-4 averaged ΔF/F0 trace of the $[Ca^{2+}]i$ changes under $H_2$-free, $H_2$-medium, and then back to $H_2$-free conditions. E. Different time period of Fluo-4 images and averaged F/F0 traces in $H_2$-induced MSCs $[Ca^{2+}]i$ during extended time-lapse imaging. F. Time-lapse $Ca^{2+}$ images and Fluo-4 averaged F/F0 trace of MSCs under $H_2$-free, $H_2$-medium (Saturated $H_2$ medium), 1/2$H_2$-medium, and 1/4$H_2$ medium. G & H, Pseudocolor (G left) and time series (G right) images and the Fluo4 averaged F/F0 trace of the $[Ca^{2+}]i$ changes under $H_2$-free, $Ca^{2+}$-medium, $H_2$+$Ca^{2+}$free-medium, and then back to $H_2$-medium conditions. I & J, Pseudocolor (I left) and time series (I right) images and the Fluo4 averaged F/F0 trace of the $[Ca^{2+}]i$ changes

under $H_2$-free, 2-APB-medium, and then back to 2-APB+$H_2$-medium. K & L, Time series images and the averaged F/F0 trace of the $[Ca^{2+}]i$ changes in ER (K) and Mito (L) under $H_2$-free and $H_2$-medium. M, Co-localization of Mito-$Ca^{2+}$ and ER-$Ca^{2+}$ with their trackers, respectively. N, simplified model illustrating the promotion of $[Ca^{2+}]i$ by $H_2$ from extracellular. White arrows in A, C, E, G, and I indicate cells at distinct time points within the time-lapse capture. Sampling rate, 10 sec.

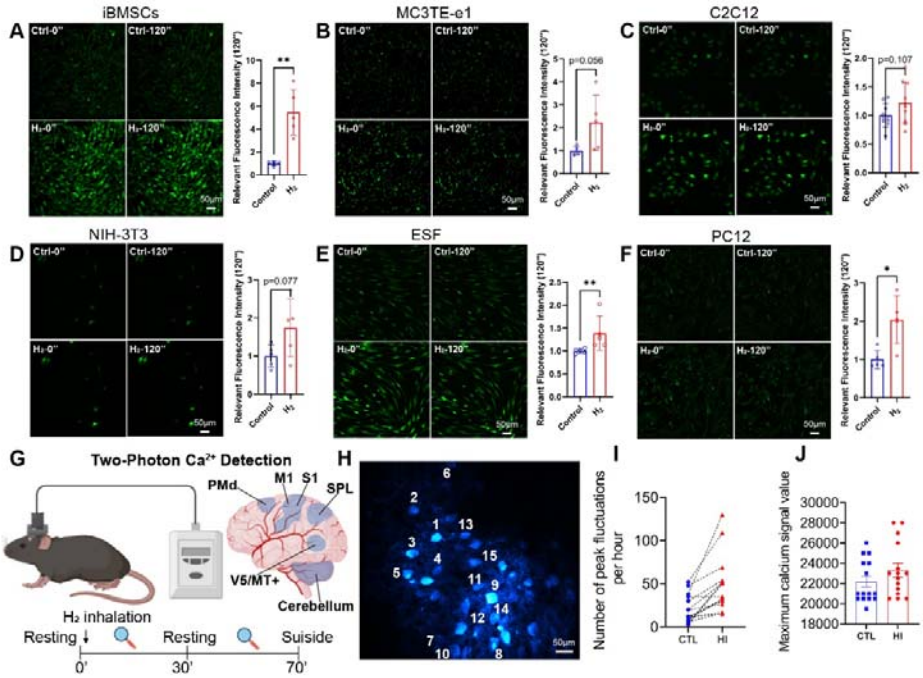


**Fig.2. In-vitro and In-vivo assays confirmed $H_2$ promoted $[Ca^{2+}]i$ in varous cells.**

A-F, $H_2$ stimulates calcium ion influx in various cells, including mouse bone marrow-derived mesenchymal stem cells (iBMSCs), mouse osteoblasts (MC3T3-E1), mouse myoblasts (C2C12), mouse fibroblasts (NIH-3T3), human skin fibroblasts (ESF), and rat neuronal cells (PC12); The left panels show random field fluorescence images of $Ca^{2+}$ at 0 and 120 seconds, respectively, and the right panels display the relative fluorescence intensity statistics at 120 seconds. G, upper left, common window of mouse brain preparations for in vivo two-photon $Ca^{2+}$ imaging; upper right, six distinct functional areas of the mouse cerebral cortex, including the monitored Primary Motor Cortex (M1) region.; lower, schematic diagram of the animal experimental procedure. H, randomly selected 15 neurons in the M1 region. I, comparison between Conctrl group (CTL) and $H_2$ inhalation group (HI) in the number of peak fluctuations per hour. J, comparison between CTL and HI groups in the maximum calcium signal value. *$p < 0.05$, **$p < 0.01$.

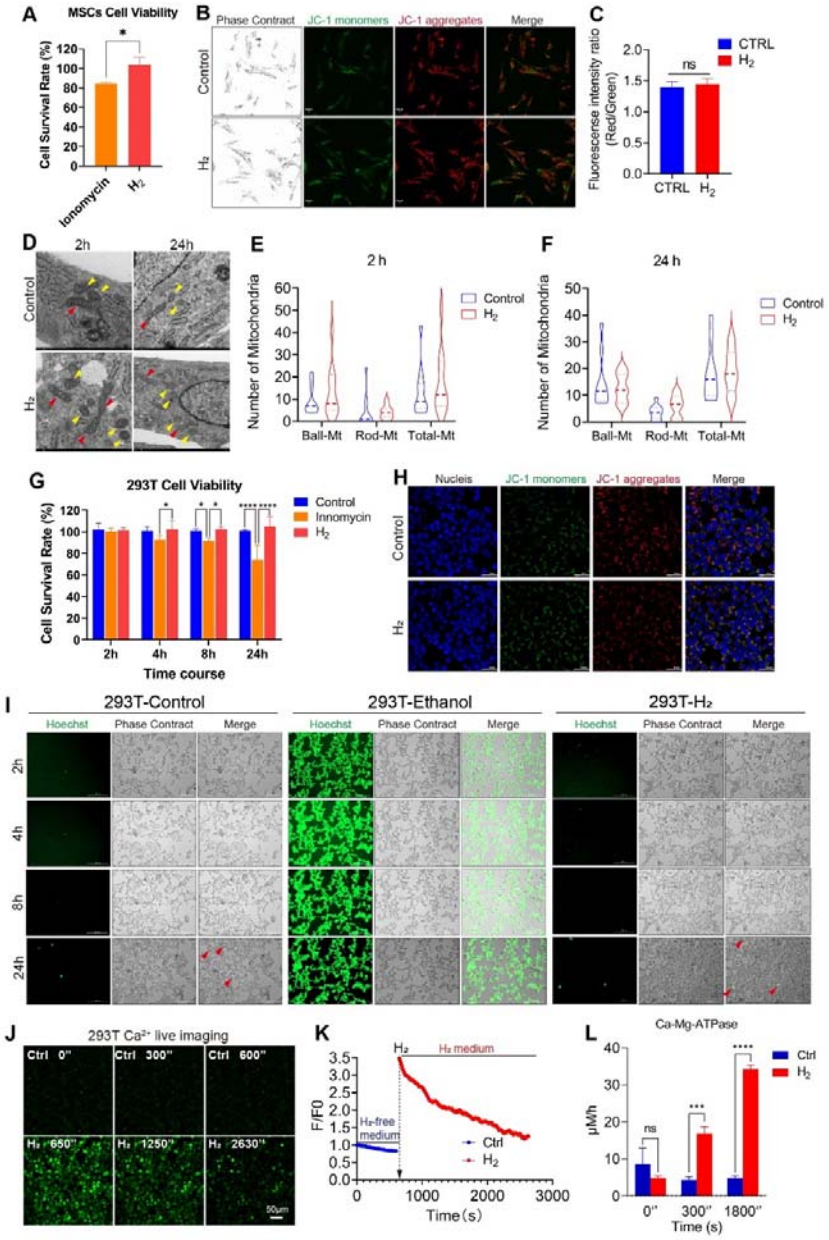


**Fig. 3. $H_2$ promotes $[Ca^{2+}]i$ without altering cellular activity or $Ca^{2+}$ overload.**

A & G, The cell viability of MSCs (A) and 293T (G) remained unaffected by $H_2$ exposure, in contrast to the significant cytotoxicity induced by the $Ca^{2+}$ ionophore Ionomycin. Mitochondrial membrane potential (MMP) measurement by JC-1 dye in B, C (MSCs) and H (293T). D, Mitochondrial morphological changes in MSCs induced by $H_2$ at 2 and 24 hours post-treatment according to the transmission electron microscopy (TEM) detection. E & F, Comparison of ball, rod-shaped, and total mitochondrial counts in MSCs after 2 and 24 hours of $H_2$ treatment. I, Live cell imaging of 293T cell death staining following 24 hours of $H_2$ treatment. J & K, Time-lapse live cell imaging of $H_2$-promoted $[Ca^{2+}]i$ dynamics and F/F0 fluorescence intensity analysis. L, Temporal analysis of Ca-Mg-ATPase activity in

293T cells following $H_2$ treatment. *p < 0.05, ***p< 0.001, ****p< 0.0001, ns: no significance.

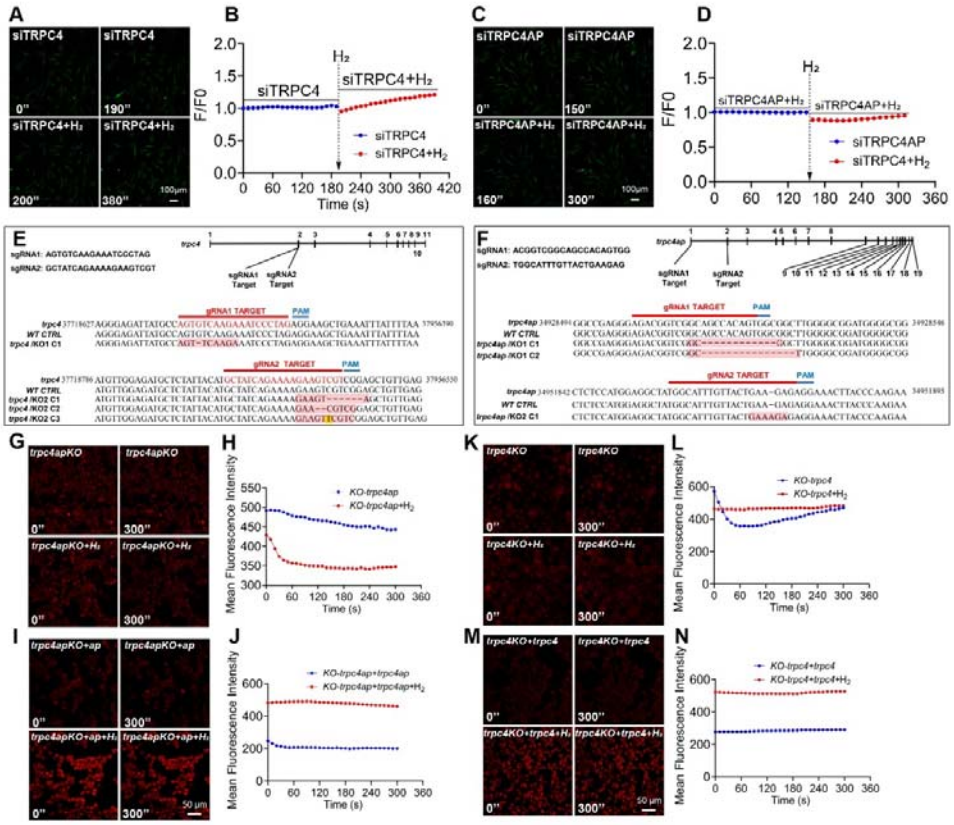


**Fig. 4. The $[Ca^{2+}]i$ induced by $H_2$ is abolished following the knockdown or knockout of *trpc4* or *trpc4ap* genes.** A & C siRNA-mediated TRPC4 and TRPC4ap knockdown abrogated the $[Ca^{2+}]i$ triggered by $H_2$. E & F, Confirmation of trpc4 and trpc4ap knockout in monoclonal 293T cell lines generated by CRISPR-Cas 9. For each sgRNA, the target sequence is shown. The mutant site is highlighted by red color, and the protospacer adjacent motif (PAM) is underlined. Sequences of knockout cells were determined by next-generation sequencing. G & K, $[Ca^{2+}]i$ induced by $H_2$ vanished following the knockout of trpc4 or trpc4 ap. I & M, $[Ca^{2+}]i$ induced by $H_2$ recovered after trpc4 or trpc4ap overexpression in the trpc4 or trpc4ap knockout cell lines. B, D, H, J, L, & N, graphs showing the Fluo4 averaged F/F0 trace of the $[Ca^{2+}]i$ changes under different conditions.

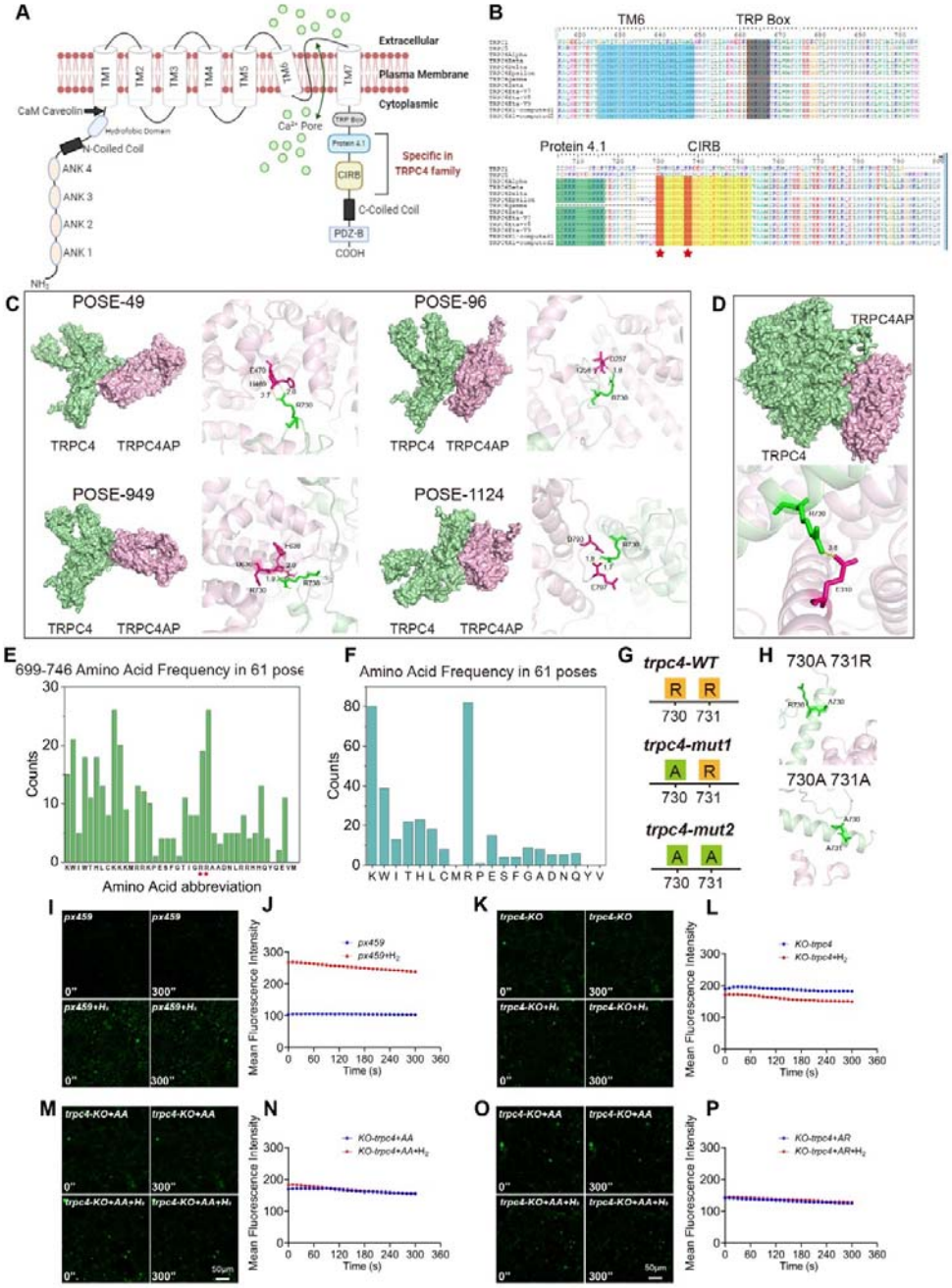


**Fig. 5. Molecular docking and mutational analyses confirm that TRPC4-TRPC4ap interaction is essential for $H_2$-induced $[Ca^{2+}]i$.** A, Diagram of the structure of an TRPC4 $Ca^{2+}$ channel including the specific motifs for TRPC4 family. B, Amino acid sequence alignment of TRPC1, TRPC5, and 11 subtypes of the TRPC4 family within the TM6, TRP Box, Protein 4.1, and CIRB domains. The specific arginine residues within the TRPC4 family are highlighted, and the areas of interest (arginine residues) in the CIRB motif are indicated by red pentagrams in the sequence alignment. C & D, Molecular docking utilizing advanced protein-docking software (C) and the AlphaFold 3 platform (D)

confirmed the interaction binding sites of TRPC4 and TRPC4ap, with consistent prediction outcomes. E & F, Amino acid frequency analysis at various positions (E) and total count (F) from the top 61 TRPC4-TRPC4ap combination patterns with the highest scores, double Arginine residues are indicated with red pentagram symbol. G, Schematic representation of the wild-type and two mutant forms of the TRPC4 protein at positions 730 and 731 at the C-terminus. H, Molecular docking utilizing the AlphaFold 3 predicted the binding affinity of two TRPC4 mutants with TRPC4ap at positions 730 and 731, indicating a loss of binding interaction. I-P, $[Ca^{2+}]i$ induced by $H_2$ and the Fluo4 averaged F/F0 trace of the $[Ca^{2+}]i$ changes under different conditions, including blank vehicle, trpc4-KO, trpc4-KO+$Arg^{730}Arg^{731}$, trpc4-KO+$Ala^{730}Arg^{731}$.

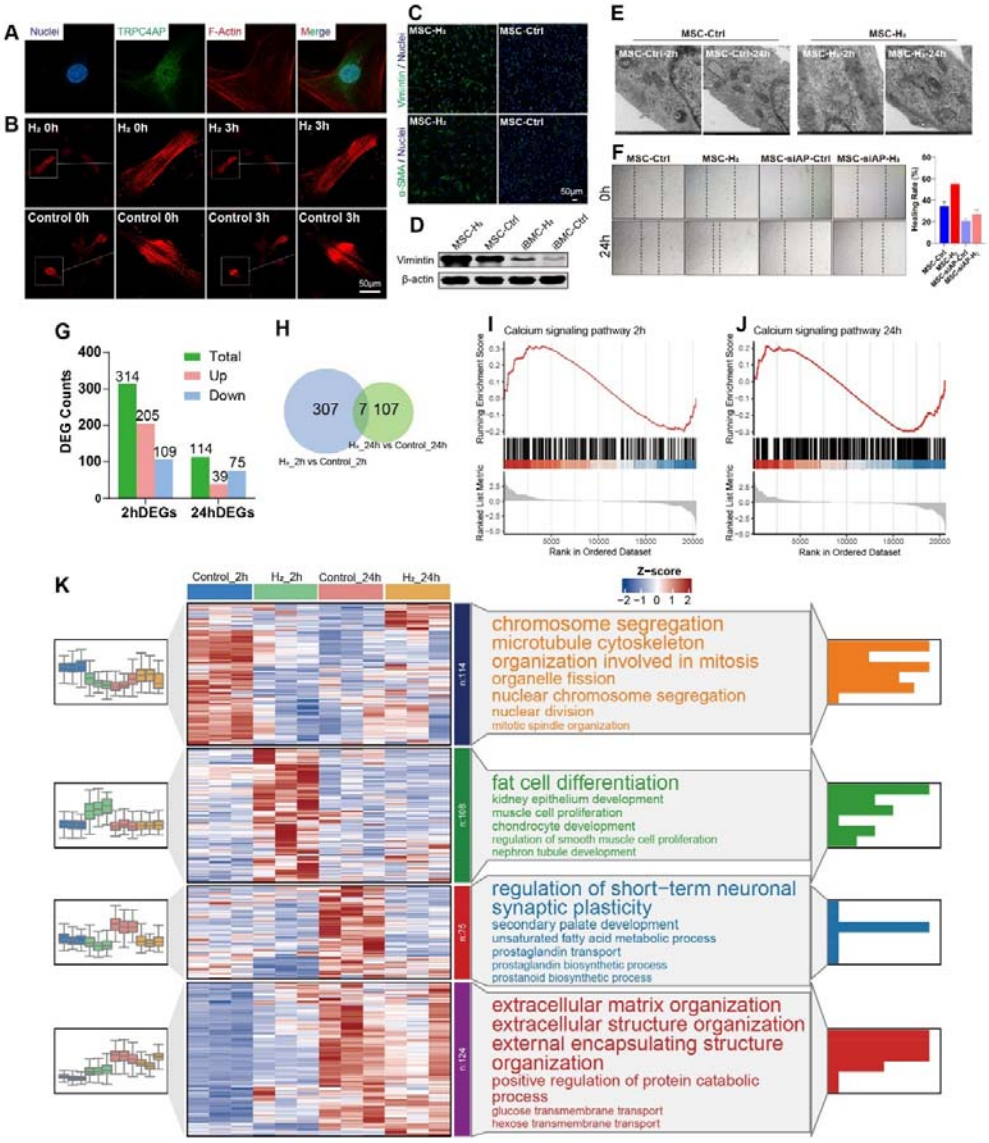


**Fig. 6. Multifaceted analysis of MSCs response to $H_2$ treatment.** A. Fluorescence co-localization results of F-Actin (red) and the TRPC4AP (green). B. Time-lapse F-Actin probes images of MSCs under $H_2$-free (Control) and $H_2$-medium. C. Immunofluorescence

results of Vimentin and α-SMA in the Control and $H_2$ groups of MSCs. D. Western Blot results of the effect of $H_2$ on Vimintin expression in MSCs and iBMCs. E. Electron microscopy results of MSCs after treatment with $H_2$ for 2 hours and 24 hours. F. Cell scratch results (left) and healing rate (right) for MSCs treated with $H_2$ for 24 hours after siRNA AP treatment. G. Counts of differentially expressed genes (DEG) in MSCs after $H_2$ treatment for 2 hours and 24 hours as revealed by RNA sequencing results. H. Venn diagram of differential genes between 2 hours and 24 hours post-treatment with $H_2$. I&J. GSEA analysis of Calcium signaling pathway in MSCs treatment 2 hours (I) and 24 hours (J) under $H_2$. K. Expression trends, heat maps, and significantly enriched Biological Process terms for each cluster of differentially expressed genes (DEGs) in MSCs; the left side depicts box plot diagrams illustrating the expression trends of DEGs across each cluster in Control and $H_2$-treated samples; the center section presents heat maps of DEGs for each cluster, with color gradients from blue to red representing increasing expression levels; the right side shows the top 6 significantly enriched pathways from GO Biological Process enrichment analysis of DEGs in each cluster, sorted by p-value, along with the corresponding bar charts.

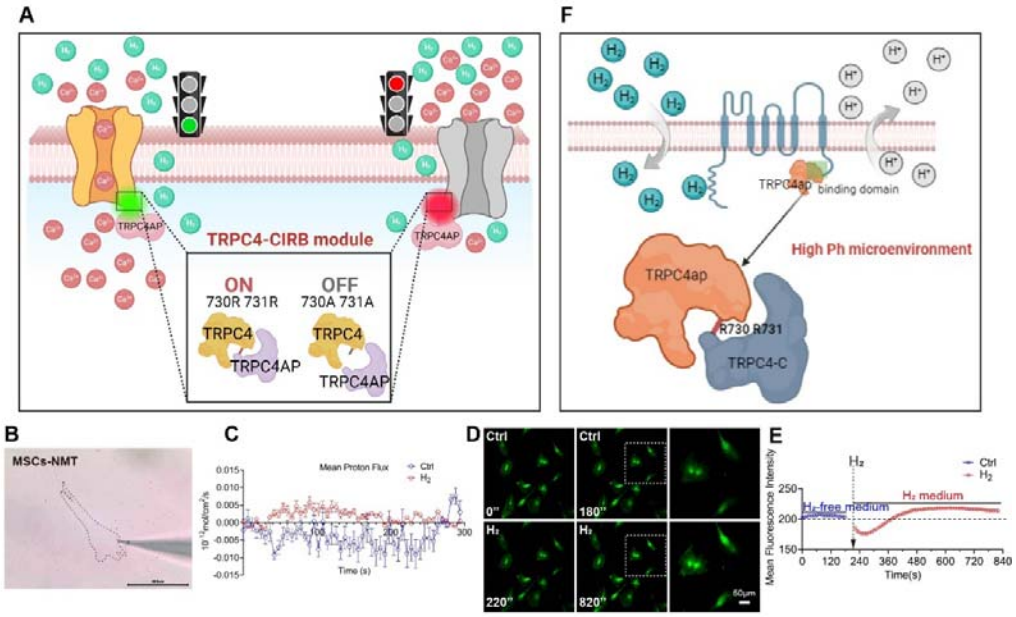


**Fig. 7. Potential molecular mechanism of $H_2$ promoting $[Ca^{2+}]i$ by acting on the TRPC4-TRPC4ap binding site.** A. Schematic representation of the $H_2$-dependent binding site of TRPC4-TRPC4ap facilitating $[Ca^{2+}]i$. B, Schematic diagram of live cell NMT detection of MSCs. C, Dynamic changes in proton flux across the plasma membrane of MSCs under the influence of $H_2$. D & E, Time-lapse imaging showing the effect of $H_2$ on intracellular pH changes and mean fluorescence intensity statistics.